

---

# ISOMORPH: A Supply Chain Digital Twin for Simulation, Dataset Generation, and Forecasting Benchmarks

---

**Zhizhen Zhang\***

University of Massachusetts Amherst  
zhizhenzhang@umass.edu

**Hyemin Gu\***

University of Massachusetts Amherst  
hgu@umass.edu

**Benjamin J. Zhang**

University of North Carolina  
bjz@unc.edu

**Daniel Elenius**

SRI International  
daniel.elenius@sri.com

**Michael Tyrrell**

SRI International  
michael.tyrrell@sri.com

**Theo J. Bourdais**

California Institute of Technology  
theo.bourdais@caltech.edu

**Houman Owhadi**

California Institute of Technology  
owhadi@caltech.edu

**Markos A. Katsoulakis<sup>†</sup>**

University of Massachusetts Amherst  
markos@umass.edu

**Tuhin Sahai<sup>†</sup>**

SRI International  
tuhin.sahai@sri.com

## Abstract

Open time-series forecasting (TSF) benchmarks cover retail, energy, weather, and traffic, but supply-chain logistics remains underserved. We introduce ISOMORPH, the first public digital twin of a multi-echelon logistics network with fully interpretable, user-configurable parameters and modular topology, demand process, and control rules. The simulator advances a directed routing graph in discrete time: demand arrives at the destination, is served from stock or recorded as backlog, and triggers replenishment through the network. By construction, the state vector tracks per-node on-hand inventory together with outstanding orders, in-transit shipments, and a smoothed demand estimate across the network, so the dynamics close as a Markov chain on a high-dimensional but tractable state space whose transition kernel acts linearly on the empirical distribution of the state. The released data reproduces the bullwhip effect—the standard empirical signature of supply-chain dynamics—at empirically consistent magnitudes, and three conservation laws structurally encoded in the Markov chain serve as verification tools when users extend the simulator with their own control rules. We release datasets at two catalogue scales ( $C=50$  and  $C=200$ ) with six scenario sweeps producing 30 additional rollouts and 20 Latin-hypercube perturbations, exhibiting dynamics largely absent from fixed TSF benchmarks: variance amplification, cascading bottlenecks, regime shifts, and cross-channel coupling through shared macro shocks. Zero-shot evaluation of four foundation models (Chronos, Moirai, TimesFM, Lag-Llama) shows MASE values exceeding public GIFT-Eval references at low-to-moderate horizons, supporting incorporation into existing benchmark datasets. The same pairing produces forecast confidence bands via Latin-hypercube perturbation of

---

\*Authors contributed equally

<sup>†</sup>Corresponding authors

demand-side knobs, a form of forward UQ from parameter uncertainty unavailable on standard TSF datasets, demonstrating that foundation models can serve as fast surrogates for the digital twin’s forward UQ. Code (MIT) is released at <https://github.com/tuhinsahai/ISOMORPH>.

**Acknowledgements.** This material is based upon work of the authors supported by the Defense Advanced Research Projects Agency (DARPA) under Agreement No. HR00112590112. Approved for public release; distribution is unlimited.

## Contents

<b>1</b>	<b>Introduction</b>	<b>3</b>
<b>2</b>	<b>Related work</b>	<b>5</b>
2.1	Time-series forecasting benchmarks . . . . .	5
2.2	Supply-chain simulators and datasets . . . . .	5
2.3	Other digital twins as ML dataset generators . . . . .	5
<b>3</b>	<b>The ISOMORPH digital twin</b>	<b>6</b>
3.1	Overview . . . . .	6
3.2	Mathematical model . . . . .	7
3.2.1	Markov chain structure . . . . .	7
3.2.2	Demand intensity . . . . .	11
3.2.3	Replenishment policy and destination service . . . . .	11
3.2.4	Inter-warehouse flows . . . . .	12
3.3	Algorithms . . . . .	13
3.3.1	Per-step algorithm . . . . .	13
3.3.2	Greedy first-fit packing . . . . .	14
3.3.3	Intensity construction algorithm . . . . .	15
<b>4</b>	<b>The right state space and its consequences</b>	<b>15</b>
4.1	Markov property . . . . .	15
4.2	Discrete conservation laws . . . . .	16
4.3	Continuous-time fluid limit: coupled transport and queueing . . . . .	17
<b>5</b>	<b>Released datasets</b>	<b>19</b>
5.1	User input configurations and output sequences . . . . .	19
5.2	Validation . . . . .	20
<b>6</b>	<b>Digital Twin meets TSF foundation models</b>	<b>21</b>
6.1	TSF benchmarking for logistics . . . . .	21
6.2	Zero-shot forward UQ from the digital twin and foundation models . . . . .	21
6.3	Results . . . . .	22
<b>7</b>	<b>Limitations and scope of claims</b>	<b>22</b>

<b>8</b>	<b>Release and maintenance</b>	<b>23</b>
<b>9</b>	<b>Conclusion and outlook</b>	<b>23</b>
<b>A</b>	<b>Parameter values</b>	<b>26</b>
A.1	Demand-generator coefficients . . . . .	26
A.2	Inventory policy and source lead times . . . . .	26
A.3	Edge transport parameters . . . . .	26
A.4	Last-mile back-solve . . . . .	26
A.5	Runtime parameters . . . . .	27
<b>B</b>	<b>Dataset schema</b>	<b>28</b>
B.1	Release overview . . . . .	28
B.2	File inventory . . . . .	28
B.3	Per-file schemas . . . . .	28
B.4	Scenario sweeps . . . . .	30
<b>C</b>	<b>Foundation model evaluation details</b>	<b>31</b>
C.1	MASE: formal definition . . . . .	31
C.2	Results at $C=200$ . . . . .	31
C.3	Lag-Llama at $L=32$ . . . . .	32
C.4	Per-horizon scenario results . . . . .	32
C.5	Models and inference hyperparameters . . . . .	32
<b>D</b>	<b>Additional results</b>	<b>33</b>
D.1	Bullwhip method . . . . .	33
D.2	Per-node bullwhip ratios . . . . .	33
D.3	Additional results on Forward UQ . . . . .	33
<b>E</b>	<b>Computational resources</b>	<b>33</b>

## 1 Introduction

Public time-series forecasting (TSF) benchmarks cover retail, energy, weather, and traffic fairly extensively. However, supply chain logistics, one of the most critical applied forecasting domains, remains underserved, with a complete lack of datasets for training and benchmarks. The closest existing resources address the domain in a limited manner. SupplyGraph [Wasi et al., 2024] provides eight months of per-product demand with a static product relationship graph from a single company. However, it has no logistics network characteristics that include inventory state, transportation edges, or capacities. DeepBullwhip [Arief, 2026] simulates a four-stage serial chain to study how demand swings amplify upstream, but releases no supply chain forecasting dataset. M5 [Makridakis et al., 2022] aggregates retail demand hierarchically by store and category. It records only what customers bought, not the warehouses, shipments, or inventory behind those sales. Across all three, the same piece is missing: demand series paired with the topology, capacities, and control decisions that determine whether the network can deliver.

Therefore, to close this gap, one needs a different kind of resource. A real-world dataset, even from a willing operator, observes one realization of a logistics network. Capacities, routing rules, and control

decisions sit implicitly inside the recorded series; they cannot be inspected, modified, or replayed under alternative settings. A simulator-based dataset makes those rules explicit: the network, the demand process, and the control policy are part of the deliverable, and the dataset is one realization of a configuration that other users can reproduce, rescale, or modify. Adjacent domains have used this perspective. BuildingsBench [Emami et al., 2023] pairs an EnergyPlus simulator with a curated load-forecasting benchmark for buildings, the most closely related work. No equivalent exists for supply-chain logistics.

This paper introduces ISOMORPH, a digital twin of a multi echelon logistics network. The user supplies a directed graph of source, intermediate, and destination nodes with edge transit times and per edge container capacities; the simulator runs the network forward at a user chosen time resolution, with shipments routed by Dijkstra, packed greedily into containers, and replenished under an  $(s, S)$  policy. The simulator’s parameters fall into two groups: *structural parameters* (topology, catalogue size  $C$ , time resolution, and horizon), which fix what dataset is being generated; and *scenario knobs* (demand structure, inventory, edge transport), which govern how the network operates within that structure. We release a family of datasets generated from one set of structural parameters—a 13-node U.S. network at daily resolution (three sources, nine warehouses across five tiers, and a destination served by two last-mile edges) at two cardinalities ( $C=50$  and  $C=200$ )—together with rollouts from perturbed scenario knobs. The simulator is fully open-source and modular: any user can swap the topology, time resolution, demand process, or control rules to generate releases tailored to their own setting. Each release includes the full state trajectory of the network, covering per item demand and on hand inventory as well as per edge shipments and utilization, so quantities like per edge saturation events and destination fill rate drops can be recovered directly from the released data without rerunning the simulator.

A central design choice of ISOMORPH is the state representation. Unlike existing resources that track only per-node demand or inventory [Wasi et al., 2024, Naik et al., 2025], the state vector carries outstanding orders, in-transit shipments, and a smoothed demand estimate alongside per-node inventory. This is the right state space: it closes the dynamics as a Markov chain whose transition kernel acts linearly on the empirical distribution of the state, and it structurally encodes three conservation laws—the discrete realization of coupled transport and queueing equations—directly into the transition function (§4).

To demonstrate ISOMORPH’s use as a forecasting benchmark, we evaluate four pretrained TSF foundation models (Chronos, Moirai, TimesFM, Lag-Llama) in a zero-shot setting. At moderate prediction horizons ( $h \geq 14$ ), MASE values exceed public GIFT-Eval reference values (Table 4), suggesting that the logistics-domain patterns in our data—such as those in Figure 4—pose challenges not covered by current benchmarks. Incorporating ISOMORPH into benchmark datasets is expected to improve foundation models’ generalization to this underrepresented domain.

## Contributions

1. **Simulator.** We introduce ISOMORPH (§3), the first public digital twin of a multi-echelon logistics network designed for TSF benchmarking, with every parameter— demand, inventory, transport, routing, and control — physically interpretable and user-configurable. The simulator is open-source and modular: topology, time resolution, demand process, replenishment policy, and routing rule are swappable without modifying the simulator code. Every parameter is documented with defaults in §3.3. The simulator closely captures the day-to-day operational logic of large supply chain entities.
2. **Empirical and structural validation.** We validate the released data on two complementary axes. *Empirically*, the data reproduce the bullwhip effect at amplification levels within the cross-industry distribution reported by Cachon et al. [2007]. *Structurally*, three pathwise conservation laws – per-node mass, global mass, and backlog conservation (Proposition 4.1) – are encoded in the transition function by the right state space design. When users add their own control rules to the simulator, these conservation laws—or adapted versions—can verify fidelity of the modified implementation.
3. **Released datasets with complex supply-chain dynamics.** We release two baseline datasets generated by ISOMORPH (§5) at cardinalities  $C=50$  and  $C=200$  ( $T=52,560$  time units, chronological 70/15/15 splits, with loaders) on a 13-node U.S. network, together with 30 scenario rollouts and 20 Latin-hypercube perturbations for forward UQ. Each release exhibits coupled dy-

namics that fixed TSF benchmarks lack: variance amplification along the supply chain (bullwhip), cascading bottlenecks when demand spikes saturate last-mile capacity, long-horizon regime shifts in demand, and cross-channel coupling through a shared macro shock  $G(t)$  that simultaneously lifts every item’s demand and propagates across the network. The full network state trajectory is released alongside, so each phenomenon is directly observable from the public files.

4. **Forward UQ on supply-chain dynamics.** The pairing of ISOMORPH with zero-shot foundation models enables forward uncertainty quantification (UQ) under perturbations that standard TSF datasets cannot expose: *parameter uncertainty* (numerical values of scenario knobs such as demand-shock intensities and drift coefficients) and *model uncertainty* (structural choices such as distributional families and replenishment policies). We perform forward UQ via a Latin-hypercube design over three demand-side knobs (§6.2, Figure 5), producing forecast envelopes (confidence bands) that allow foundation models to be evaluated on their ability to generalize under perturbations in the dynamics’ parameters.

## 2 Related work

### 2.1 Time-series forecasting benchmarks

Standard TSF suites collect real-world series across multiple domains such as electricity, weather, retail, and traffic. Common ones include **ETT** [Zhou et al., 2020], **M4** and **M5** [Makridakis et al., 2019, 2022], **Monash** [Godahehwa et al., 2021], and the recent **GIFT-Eval** [Aksu et al., 2024]. The **Time-Series-Library** [Wu et al., 2024] is a code library of TSF model implementations and evaluation tooling, not a benchmark. None of these releases include the data-generating process: users cannot change parameters or regenerate the data under alternative settings. Synthetic priors such as **KernelSynth** [Ansari et al., 2024] and **ForecastPFN** [Dooley et al., 2023] are tunable, but their parameters describe abstract mathematical models rather than physically interpretable quantities. ISOMORPH differs from both: it is synthetic, but every parameter corresponds to a physical operational quantity in a multi-echelon logistics network.

### 2.2 Supply-chain simulators and datasets

Public supply-chain forecasting resources are limited. **SupplyGraph** [Wasi et al., 2024], the only real-data release, provides eight months of SKU-level demand from one FMCG company, with no logistics topology. Open-source simulators target inventory policy and bullwhip dynamics rather than standalone TSF benchmarking: **deepbullwhip** [Arief, 2026] provides a serial-chain simulator with a collection of forecasting methods evaluated on bullwhip metrics, and **OR-Gym** [Hubbs et al., 2020] packages multi-echelon inventory as RL environments. **BULL-ODE** [Naik et al., 2025] forecasts coupled inventory–order–demand trajectories from a single-echelon continuous-time testbed under three synthetic demand regimes. All three fix the topology to a serial or single-tier chain, and none releases a TSF benchmark in the style of GIFT-Eval or Monash. Hierarchical retail releases such as **M5** [Makridakis et al., 2022] have a location hierarchy but no transport network with capacity constraints, so they cannot expose the network-state dynamics that drive bottleneck and fill-rate behavior in ISOMORPH.

### 2.3 Other digital twins as ML dataset generators

Pairing a simulator with a forecasting benchmark has been done in other fields. **Buildings-Bench** [Emami et al., 2023] pairs the EnergyPlus building simulator with a benchmark for short-term electricity load forecasting. **ClimateBench** [Watson-Parris et al., 2022] trains ML models to emulate CMIP6 climate model output, which is a distinct task from time-series forecasting. ISOMORPH brings the same pairing to supply chains and extends it with zero-shot foundation-model evaluation under parameter perturbations; to our knowledge, this is the first such computational methodology for multi-echelon logistics.

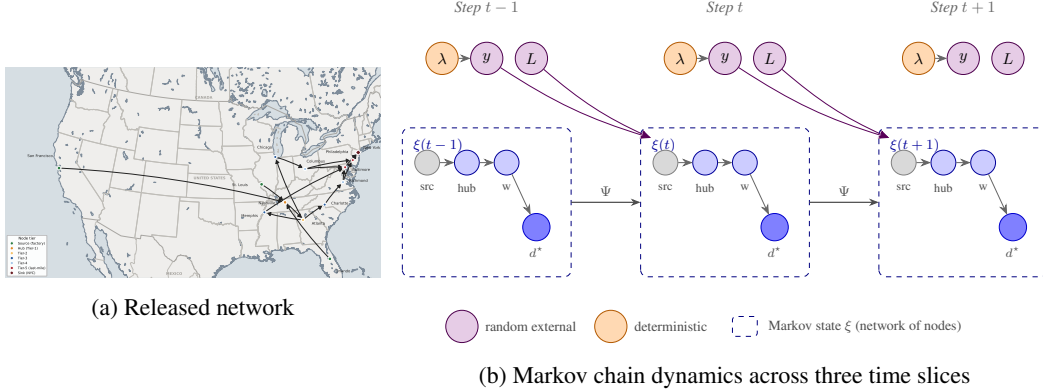


Figure 1: The ISOMORPH model. **(a)** Released network: 13 U.S. cities (3 sources, 9 intermediate warehouses across 5 tiers, and destination New York) connected by 16 directed edges, each carrying a user-set transit time  $\tau_e$ ; the map shows geographic placement, but the graph structure and routing are defined by the edges and their transit times, not by geographic distance. **(b)** Dynamic Bayesian network across three time slices. Top row: random inputs—demand  $y_t$  (violet, drawn from deterministic intensity  $\lambda_t$ , orange) and source lead times  $L_t$  (violet). Bottom row (dashed boxes): Markov state  $\xi_t$  transitioned by  $\Psi$  (Algorithm 1), see also Fig. 2 Each slice shows a representative subset of the  $|\mathcal{N}| = 13$  nodes (cities).

### 3 The ISOMORPH digital twin

#### 3.1 Overview

ISOMORPH simulates the flow of *multiple item types* (a catalogue of  $C$  goods) through a *directed network* of factories, intermediate warehouses, and a customer-facing destination, advancing the state of every location and link forward in *discrete time* at user-prescribed time resolution (day/hour/minute). In a single rollout, random customer demand arrives at the destination each step, is served from available stock, and triggers replenishment through the network; the cycle repeats. At the end of each step  $t$  the simulator collects the state of the entire network—stock levels at each location for each of the  $C$  items, unfilled orders, in-transit shipments, and a smoothed demand estimate—into a single vector  $\xi_t$  (formal definition in §3.2.1, Eq. 1).

The network is a user-supplied directed graph  $\mathcal{G} = (\mathcal{N}, \mathcal{E})$  whose locations are embedded in two-dimensional geography (e.g. U.S. cities); however, the metric on this graph is defined by user-set integer transit times  $\tau_e$  on each link, not by geographic distance. Locations split into three roles: factories  $\mathcal{N}_{\text{src}}$  with unbounded upstream supply, intermediate warehouses  $\mathcal{N}_{\text{int}}$ , and a customer-facing destination  $d^*$ . Each directed link  $e = (u, v)$  carries, in addition to  $\tau_e$ , a per-container volume  $V_e$  and a per-step container count  $K_e$ , giving volume capacity  $K_e V_e$  per step. Dijkstra’s algorithm routes shipments over these transit times, so the user controls both the topology and the effective distances by choosing which locations to connect and what  $\tau_e$  to assign (Figure 1(a); §3.2.1; released values in Appendix A.3, Table 7).

The dynamics is modeled as a *Markov chain*: the sequence of state variables  $\{\xi_t\}$  satisfies  $\xi_{t+1} = \Psi(\xi_t, y_t, L_t)$ , where  $\Psi$  is a deterministic transition function driven by two random inputs—exogenous Poisson customer demand  $y_t$  and Gaussian factory lead times  $L_t$ , the latter drawn conditioned on  $\xi_t$  at source locations whose stock falls below a reorder threshold. The demand  $y_t$  is generated from a five-component intensity combining seasonality, drift, bursts, and a shared macro shock (§3.2.2). Figure 1(b) shows the Markov chain unrolled over three time slices. The physical rules that constitute  $\Psi$  are organized into two groups: replenishment and service rules (§3.2.3), which govern when each location reorders stock and how the destination serves or backlogs demand; and inter-warehouse flows (§3.2.4), which specify source arrivals, Dijkstra-based dispatch, and inter-warehouse pulls, see Figure 2. The state space, the random inputs, the transition map  $\Psi$ , and the resulting transition kernel are specified in §3.2.1 (Eqs. 9–10).

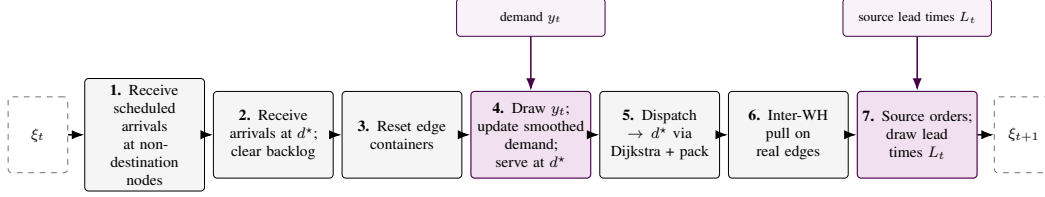


Figure 2: One-step transition map  $\Psi : \xi_t \mapsto \xi_{t+1}$  as a fixed sequence of seven sub-steps (Algorithm 1). Random external inputs (violet, top) enter at exactly two sub-steps—demand  $y_t$  at sub-step (4) and source lead times  $L_t$  at sub-step (7); the remaining five sub-steps are deterministic bookkeeping given  $(\xi_t, y_t, L_t)$ . Sub-steps (1) and (2) integrate inbound arrivals due at  $t$ , (3) replenishes per-step edge capacity, (4) consumes the demand draw and updates the destination’s stock and backlog, (5) and (6) move units along edges via Dijkstra routing and greedy first-fit packing, and (7) places fresh source orders with stochastic lead times.

Our model assumes stationary topology, fixed control policy, and deterministic edge transit within any run (§3.2.3). Based on these assumptions, two conservation laws – over physical units and over demand events – hold on every sample path; they are stated and proved in §4.2.

The simulator is realized as three algorithms in §3.3. The top-level procedure is Algorithm 1 (§3.3.1), a seven-stage per-step loop that defines  $\Psi$ , see Figure 2; it calls two subroutines:

- Algorithm 2 (§3.3.2): greedy first-fit packing of units into finite-capacity containers along a shipping path.
- Algorithm 3 (§3.3.3): sampling of the five-component demand intensity tensor.

## 3.2 Mathematical model

This section specifies the simulator as a mathematical object: the Markov chain structure (§3.2.1), the demand intensity (§3.2.2), the replenishment and service rules (§3.2.3), and the inter-warehouse flows (§3.2.4).

### 3.2.1 Markov chain structure

This section presents the simulator as a Markov chain. §3.2.1 declares the state space, see Figure 1. §3.2.1 specifies the random external inputs that drive each transition. §3.2.1 introduces the transition map  $\Psi$  as a measurable function. §3.2.1 defines the transition kernel as the average of the deterministic transition over the random external inputs. §3.2.1 establishes the Markov property and notes the equivalent **Dynamic Bayesian Network** (DBN) representation.

**Notation and state space** **Graph and node attributes.** Let  $\mathcal{G} = (\mathcal{N}, \mathcal{E})$  be a directed graph with  $|\mathcal{N}| = 13$ . The nodes split into three groups: source nodes  $\mathcal{N}_{\text{src}}$ , intermediate nodes  $\mathcal{N}_{\text{int}}$ , and a single destination  $d^*$ , see Figure 1. Each edge  $e = (u, v) \in \mathcal{E}$  carries a transit time  $\tau_e \in \mathbb{Z}_{\geq 1}$  (time units), a per-container volume  $V_e \in \mathbb{R}_{>0}$ , and a per-step container count  $K_e \in \mathbb{Z}_{\geq 0}$ . The per-step volume capacity on  $e$  is  $C_e := K_e V_e$ .

In the released instantiation (§3.1),  $\mathcal{N}_{\text{src}} = \{\text{San Francisco, St. Louis, Orlando}\}$ ,  $d^* = \text{New York}$ , and  $\mathcal{N}_{\text{int}}$  contains the nine intermediate warehouses; the per-edge values  $(\tau_e, V_e, K_e)$  are listed in Table 7 (§A.3).

**Items and time.** The item set is  $\mathcal{I} = \{1, \dots, C\}$  with per-item unit volumes  $v_i \in \mathbb{R}_{>0}$ . Time is discrete with one step per user-chosen time unit,  $t \in \{0, 1, \dots, T-1\}$  and horizon  $T = 52,560$ .

**State variables.** The state at the end of time unit  $t$  is the vector

$$\xi_t = (\text{OH}_t, B_t, \text{Out}_t, \text{IT}_t, \tilde{\lambda}_t) \in \mathcal{X}, \quad (1)$$

with the following five components:

- On-hand inventory  $\text{OH}_t = (\text{OH}_t^{n,i})_{n \in \mathcal{N}, i \in \mathcal{I}} \in \mathbb{Z}_{\geq 0}^{|\mathcal{N}| \times C}$ , where  $\text{OH}_t^{n,i}$  is the number of units of item  $i$  held at node  $n$ .

- Backlog  $B_t = (B_t^{n,i})_{n \in \mathcal{N}, i \in \mathcal{I}} \in \mathbb{Z}_{\geq 0}^{|\mathcal{N}| \cdot C}$ , where  $B_t^{n,i}$  is the number of demand units owed by node  $n$  for item  $i$ . Non-zero only at  $n = d^*$ .
- Outstanding source orders  $\text{Out}_t = (\text{Out}_t^{n,i})_{n \in \mathcal{N}, i \in \mathcal{I}}$ , where each  $\text{Out}_t^{n,i} \in \{\emptyset\} \cup (\mathbb{Z}_{>0} \times \mathbb{Z}_{>0})$  is either empty or a pair  $(\tau, q)$  recording  $q$  units due to arrive at time unit  $\tau$ .
- Scheduled destination arrivals  $\text{IT}_t \in \mathcal{M}(\mathbb{Z}_{>0} \times \mathcal{I} \times \mathbb{Z}_{>0})$ , a finite collection of triples  $(\tau, i, q)$  recording shipments en route to  $d^*$ .
- Smoothed demand estimate  $\tilde{\lambda}_t = (\tilde{\lambda}_t^i)_{i \in \mathcal{I}} \in \mathbb{R}_{>0}^C$ , an exponentially weighted moving average of recent observed demand, updated by  $\tilde{\lambda}_{t+1}^i = \alpha y_{i,t} + (1 - \alpha) \tilde{\lambda}_t^i$  with  $\alpha = 0.05$ .

**Hybrid state space.** The state  $\xi_t$  combines four discrete-valued components and one continuous-valued component. The discrete part lives in

$$\mathcal{Q} = \mathbb{Z}_{\geq 0}^{|\mathcal{N}| \cdot C} \times \mathbb{Z}_{\geq 0}^{|\mathcal{N}| \cdot C} \times (\{\emptyset\} \cup \mathbb{Z}_{>0} \times \mathbb{Z}_{>0})^{|\mathcal{N}| \cdot C} \times \text{Lists}(\mathbb{Z}_{>0} \times \mathcal{I} \times \mathbb{Z}_{>0}),$$

a countable set comprising integer counts for on-hand inventory and backlog ( $|\mathcal{N}| \cdot C$  entries each), optional integer pairs for outstanding source orders ( $|\mathcal{N}| \cdot C$  entries), and a finite list of triples  $(\tau, i, q)$  recording shipments scheduled to arrive at  $d^*$  at time unit  $\tau$ . The continuous part is the smoothed demand vector  $\tilde{\lambda}_t \in \mathbb{R}_{>0}^C$ , which takes values in a  $C$ -dimensional positive-real space. The full state space is the hybrid product

$$\mathcal{X} = \mathcal{Q} \times \mathbb{R}_{>0}^C, \quad (2)$$

on which probability distributions are defined in the standard way for hybrid spaces (the Borel product of the discrete  $\sigma$ -algebra on  $\mathcal{Q}$  with the Borel  $\sigma$ -algebra on  $\mathbb{R}_{>0}^C$ ).

**Per-edge in-transit volumes (derived quantity).** Per-edge in-transit counts are not part of the state variables above. We write  $q_{i,t}^{u \rightarrow v}$  for the cumulative count of item- $i$  units on edge  $(u, v)$  at the end of time unit  $t$ , computed as the sum of all dispatches that have been routed onto  $(u, v)$  but whose realized arrival time is strictly later than  $t$ . This is a derived quantity, reconstructible from the dispatch records produced inside the per-step update (Algorithm 2, §3.3.2); it is referenced in Proposition 4.1.

**Random external inputs.** At each step  $t$ , the per-step update reads two random vectors  $(y_t, L_t)$  that are external inputs, supplied to the system rather than computed from its current state. They are not part of the state.

**Demand.** The demand vector  $y_t = (y_{1,t}, \dots, y_{C,t}) \in \mathbb{Z}_{\geq 0}^C$  has independent Poisson components,

$$y_{i,t} \sim \text{Poisson}(\lambda_{i,t}), \quad (3)$$

with the draws independent across both  $i$  and  $t$ . The intensity sequence  $(\lambda_{i,t})_{i \in \mathcal{I}, t \in \{0, \dots, T-1\}}$  is constructed in §3.2.2 (see (14)) and §3.3.3 (algorithmic construction). For the present subsection,  $(\lambda_{i,t})$  is treated as a fixed input to the chain.

**Source lead times.** Define the set of source-item pairs that need a fresh order on a state  $\xi$  as

$$\mathcal{T}(\xi) = \{(n, i) \in \mathcal{N}_{\text{src}} \times \mathcal{I} : \text{OH}^{n,i} < s^{n,i}, \text{Out}^{n,i} = \emptyset\}, \quad (4)$$

where the parameters  $(s^{n,i}, \mu^{n,i})$  are specified in §3.2.3. For each  $(n, i) \in \mathcal{N}_{\text{src}} \times \mathcal{I}$ , define

$$L_t^{n,i} = \max(1, \lceil X_t^{n,i} \rceil), \quad X_t^{n,i} \sim \mathcal{N}(\mu^{n,i}, (0.2 \mu^{n,i})^2). \quad (5)$$

Writing  $\Phi$  for the standard-Gaussian cumulative distribution function, the integer  $L_t^{n,i}$  takes value  $\ell$  with probability

$$\mathbb{P}(L_t^{n,i} = \ell) = \begin{cases} \Phi\left(\frac{1 - \mu^{n,i}}{0.2 \mu^{n,i}}\right), & \ell = 1, \\ \Phi\left(\frac{\ell - \mu^{n,i}}{0.2 \mu^{n,i}}\right) - \Phi\left(\frac{\ell - 1 - \mu^{n,i}}{0.2 \mu^{n,i}}\right), & \ell \geq 2. \end{cases} \quad (6)$$

Collect all draws into the lead-time vector

$$L_t = (L_t^{n,i})_{(n,i) \in \mathcal{N}_{\text{src}} \times \mathcal{I}} \in \mathbb{Z}_{\geq 1}^{|\mathcal{N}_{\text{src}}| \cdot C}. \quad (7)$$

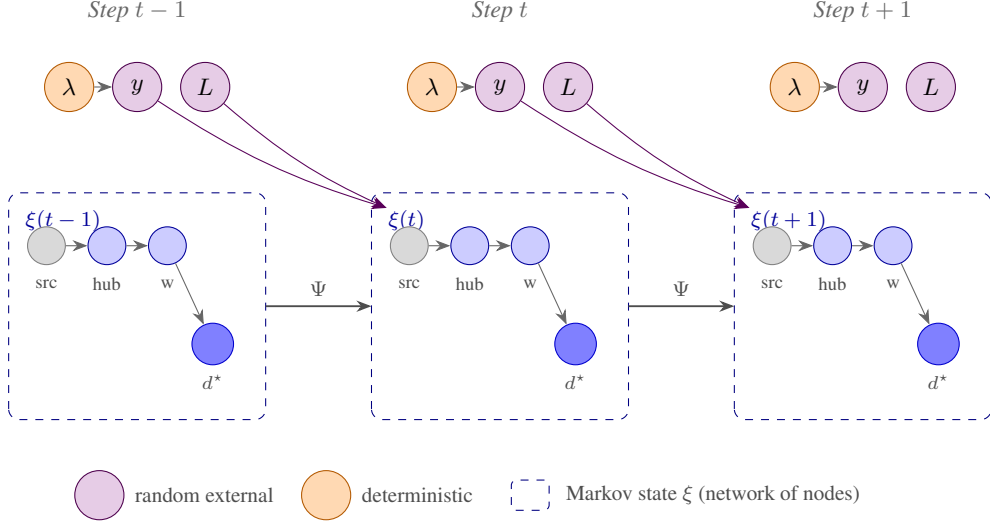


Figure 3: The ISOMORPH model as a dynamic Bayesian network across three time slices. *Random external inputs* (top row, violet): demand  $y_t \sim \text{Poisson}(\lambda_{i,t})$  and source lead times  $L_t$  are the only sources of randomness in the chain. The intensity  $\lambda$  (orange) is deterministic given the simulator seed. *Markov state* (bottom row, dashed boxes): the state  $\xi_t$  is the joint state of the simulator, transitioned by the deterministic map  $\Psi$  defined in Algorithm 1. The illustrated nodes inside each slice are organized by the partition  $\mathcal{N} = \mathcal{N}_{\text{src}} \sqcup \mathcal{N}_{\text{int}} \sqcup \{d^*\}$  from §3.2.1: a representative source, two intermediate nodes (a hub and a downstream warehouse), and the destination. We do not draw all 13 cities of the released topology in each slice; the figure shows the role of each group, not the full graph. The geographic instantiation ( $\mathcal{N}_{\text{src}} = \{\text{San Francisco, St. Louis, Orlando}\}$ ,  $d^* = \text{New York}$ , and the nine intermediate nodes) is in Figure 1 of the main text.

The transition map  $\Psi$  in §3.2.1 reads only the components indexed by  $\mathcal{T}(\xi_t)$ ; the remaining components are extra randomness that has no effect on  $\xi_{t+1}$ .

**Independence and initialization.** Conditional on  $\xi_t$ , the lead-time vector  $L_t$  has independent components and is independent of  $y_t$ . The collection  $((y_t, L_t))_{t \geq 0}$  is jointly independent across  $t$ . The initial state  $\xi_0 \in \mathcal{X}$  is fixed in advance, specified by the simulator configuration. Throughout this paper, the simulation seed is treated as a fixed parameter; randomness in the chain comes only from  $((y_t, L_t))_{t \geq 0}$ .

**One-step transition map.** The transition from  $\xi_t$  to  $\xi_{t+1}$  has two layers. The first is a deterministic map  $\Psi$  that, given the current state and a realized draw of the random external inputs, computes the next state by mechanical bookkeeping. The second is the transition probability  $P_t$  obtained by averaging  $\Psi$  over the distribution of those inputs. This subsection specifies  $\Psi$ ; §3.2.1 specifies  $P_t$ .

Define  $\Psi$  as the composition of the seven sub-step operations of Algorithm 1 (§3.3.1), executed in fixed order, viewed as a map

$$\Psi : \mathcal{X} \times \mathbb{Z}_{\geq 0}^C \times \mathbb{Z}_{\geq 1}^{|\mathcal{N}_{\text{src}}| \cdot C} \longrightarrow \mathcal{X}. \quad (8)$$

Given  $\xi_t$  and realized inputs  $(y_t, L_t)$ , the next state is

$$\xi_{t+1} = \Psi(\xi_t, y_t, L_t) \quad (9)$$

deterministically: there is no further randomness in the transition once  $(y_t, L_t)$  are fixed. The seven sub-steps execute in the order specified by Algorithm 1, and the resulting state  $\xi_{t+1}$  depends on this ordering. Each sub-step is built from arithmetic operations, indicator functions, and finite enumeration over the finite sets  $\mathcal{N}$ ,  $\mathcal{I}$ ,  $\mathcal{E}$ . Writing  $\Psi$  in closed form would require inlining all seven sub-steps with their (s,S) trigger logic and packing-residual dependencies into one expression; the algorithmic specification of Algorithm 1 is more compact and is the definition of  $\Psi$  throughout this paper.

**Transition probability.** The transition probability defined as

$$P_t(\xi, A) = \mathbb{P}(\xi_{t+1} \in A \mid \xi_t = \xi)$$

is constructed from  $\Psi$  in three steps: fix the realized inputs and apply  $\Psi$  deterministically, ask whether the result lands in  $A$ , then average over the distribution of inputs.

**Step 1 — pointwise transition.** For  $\xi_t = \xi$  and realizations  $(y, \ell)$ , the next state is  $\xi_{t+1} = \Psi(\xi, y, \ell)$  (§3.2.1).

**Step 2 — conditional law of inputs.** By §3.2.1, the joint conditional distribution of  $(y_t, L_t)$  given  $\xi_t = \xi$  factorizes as  $\pi_t^{\text{dem}}(y) \pi_t^{\text{lt}}(\ell)$ , with neither factor depending on  $\xi$ .

**Step 3 — average over inputs.** For each  $t \geq 0$ ,  $\xi \in \mathcal{X}$ , and event  $A$ ,

$$P_t(\xi, A) = \sum_{y \in \mathbb{Z}_{\geq 0}^C} \sum_{\ell \in \mathbb{Z}_{\geq 1}^{|\mathcal{N}_{\text{src}}| \cdot C}} \mathbf{1}\{\Psi(\xi, y, \ell) \in A\} \pi_t^{\text{dem}}(y) \pi_t^{\text{lt}}(\ell), \quad (10)$$

where

$$\pi_t^{\text{dem}}(y) = \prod_{i=1}^C \frac{\lambda_{i,t}^{y_i} e^{-\lambda_{i,t}}}{y_i!}, \quad \pi_t^{\text{lt}}(\ell) = \prod_{(n,i) \in \mathcal{N}_{\text{src}} \times \mathcal{I}} \mathbb{P}(L^{n,i} = \ell^{n,i}), \quad (11)$$

and the lead-time mass function is given in (6).

Summing over the entire state space,  $P_t(\xi, \mathcal{X}) = \sum_y \pi_t^{\text{dem}}(y) \sum_\ell \pi_t^{\text{lt}}(\ell) = 1$ , since both factors are probability mass functions and  $\Psi$  takes values in  $\mathcal{X}$ . For each fixed  $\xi$ ,  $P_t(\xi, \cdot)$  is a probability distribution over the next state.

The function  $P_t : \mathcal{X} \times \mathcal{B}(\mathcal{X}) \rightarrow [0, 1]$  is also called a *Markov transition kernel* in the probability literature. We use “transition probability” throughout to mean the same object in less technical language.

**Markov property** The Markov property compares the conditional distribution of  $\xi_{t+1}$  given the entire past against the conditional distribution given only the current state. To formalize “the entire past,” let  $\mathcal{F}_t$  be the collection of events whose outcomes are fully determined by the initial state  $\xi_0$  and the random external inputs through time unit  $t - 1$ :

$$\mathcal{F}_t = \sigma(\xi_0, y_0, \ell_0, \dots, y_{t-1}, \ell_{t-1}).$$

Concretely,  $\mathcal{F}_t$  is the set of all yes-or-no questions whose answer can be read off from the values of these inputs alone — “did inventory at warehouse  $w$  exceed 100 units yesterday?”, “has any backlog accumulated at  $d^*$  in the first week?”, and so on. Closing this set under the natural operations on events (union, intersection, complement) gives the formal object  $\mathcal{F}_t$  (a  $\sigma$ -algebra). Since  $\xi_t$  is computed from these inputs by repeated application of  $\Psi$ , any event involving  $\xi_t$  belongs to  $\mathcal{F}_t$ .

By construction,  $(y_t, L_t)$  is independent of  $\mathcal{F}_t$ , so back in (10)

$$\mathbb{P}(\xi_{t+1} \in A \mid \mathcal{F}_t) = P_t(\xi_t, A) \quad \text{a.s.} \quad (12)$$

The conditional distribution of  $\xi_{t+1}$  given the past depends on the past only through  $\xi_t$ . The chain  $(\xi_t)_{t \geq 0}$  is therefore a time-inhomogeneous Markov chain on  $\mathcal{X}$  with transition probabilities  $(P_t)_{t \geq 0}$ , where time-inhomogeneity comes from the time-varying demand intensity  $\lambda_{i,t}$  that enters  $\pi_t^{\text{dem}}$ . The augmented process  $((t, \xi_t))_{t \geq 0}$  on  $\mathbb{Z}_{\geq 0} \times \mathcal{X}$  is time-homogeneous, with transition probability

$$\bar{P}((t, \xi), \{t+1\} \times A) = P_t(\xi, A). \quad (13)$$

The state space  $\mathcal{X} = \mathcal{Q} \times \mathbb{R}_{>0}^C$  is hybrid: transitions on the continuous component  $\tilde{\lambda}$  are deterministic given  $y_t$ , while transitions on the discrete component are random.

**DBN representation.** The chain admits an equivalent representation as a dynamic Bayesian network (DBN). In this representation, the state  $\xi_t$  is decomposed into its per-node, per-item components

$$(\text{OH}_t^{n,i}, B_t^{n,i}, \text{Out}_t^{n,i}, \text{IT}_t, \tilde{\lambda}_t^i)_{n \in \mathcal{N}, i \in \mathcal{I}},$$

and the random external inputs  $(y_t, L_t)$  enter as separate input nodes, see also Figure 1. The network topology  $\mathcal{G}$  is then embedded in the cross-node dependencies within each time slice:  $\text{OH}_{t+1}^{n,i}$  depends on  $\text{OH}_t^{u,i}$  for upstream neighbours  $u$  via the inter-warehouse flows of §3.2.4. We do not use the DBN representation in the present work — the Markov chain abstraction over  $\xi_t$  is sufficient for the formal claims of §4.2 and the algorithmic specification of §3.3. The DBN view could be useful for follow-up work on inference, structure learning, or interventional reasoning.

### 3.2.2 Demand intensity

This section gives the equational form of the demand intensity sequence  $(\lambda_{i,t})$  used in §3.2.1 as the rate parameter of the Poisson demand draws.

For each item  $i$  and time unit  $t$ , demand intensity is

$$\lambda_{i,t} = \bar{\lambda}_i \cdot [1 + S_i(t) + W_i(t) + A_i(t) + P_i(t) + g_i G(t)]_{\geq \varepsilon}, \quad (14)$$

with  $[\cdot]_{\geq \varepsilon} := \max(\cdot, \varepsilon)$  and  $\varepsilon = 0.08$  (a floor that prevents the intensity from collapsing to zero). The five components are as follows.

**Yearly seasonal** (with second harmonic, so the shape is not a perfect sine):

$$S_i(t) = a_{1,i}^{(y)} \sin(\omega_y t + \phi_i) + a_{2,i}^{(y)} \sin(2\omega_y t + 0.7 \phi_i), \quad \omega_y = 2\pi/365. \quad (15)$$

**Weekly seasonal:**

$$W_i(t) = a_i^{(w)} \sin(\omega_w t + \psi_i), \quad \omega_w = 2\pi/7. \quad (16)$$

**Long-horizon drift, autoregressive of order 1 (AR(1)) and clipped:**

$$A_i(t) = \text{clip}(\phi_i^{\text{AR}} A_i(t-1) + \epsilon_{i,t}, \pm 0.6), \quad \epsilon_{i,t} \sim \mathcal{N}(0, \sigma_{\text{AR},i}^2). \quad (17)$$

The AR(1) recursion produces a slowly varying random trajectory whose persistence is set by  $\phi_i^{\text{AR}}$  and whose noise level is set by  $\sigma_{\text{AR},i}$ ; the clip at  $\pm 0.6$  keeps the drift contribution bounded.

**Per-item bursts:**

$$P_i(t) = \sum_k h_{i,k}^P \pi\left(\frac{t - t_{i,k}^P}{\Delta_{i,k}^P}\right), \quad (18)$$

where  $\pi(\cdot)$  is a trapezoidal pulse: it ramps linearly up over the first 15% of its duration, plateaus for 60%, and ramps down over the last 25%. Bursts fire as a sparse random process per item.

**Shared macro-shock:**

$$G(t) = \sum_k h_k^G \pi\left(\frac{t - t_k^G}{\Delta_k^G}\right), \quad (19)$$

drawn once per run and shared across all items, with per-item sensitivity  $g_i$ . The distributions of all coefficients are given in Table 5 (§A.1).

### 3.2.3 Replenishment policy and destination service

This section specifies the per-node replenishment policy and the destination service rule. The parameters  $(s^{n,i}, S^{n,i}, \mu^{n,i})$  are used in §3.2.1 (the trigger set  $\mathcal{T}$  and lead-time means) and in §3.3.1 (sub-step (vii)). Standing assumptions held fixed across all releases are recorded at the end.

**Replenishment.** Replenishment follows an  $(s, S)$  policy at every non-destination node: when on-hand drops below the reorder threshold  $s$ , place an order that brings on-hand back up to the order-up-to level  $S$ . The two node types realize this policy differently. Source nodes  $n \in \mathcal{N}_{\text{src}}$  act as factories with unlimited upstream supply: when  $\text{OH}^{n,i} < s^{n,i}$  and no order is outstanding, an order of size  $S^{n,i} - \text{OH}^{n,i}$  is placed and arrives after a random lead time  $L^{n,i}$  drawn as in (5). Intermediate nodes  $n \in \mathcal{N}_{\text{int}}$  use the same trigger but pull inventory from upstream neighbours along real edges; the requested quantity is physically routed and packed (Algorithm 2, §3.3.2), and the arrival time equals the realized path-transit time. Only the source boundary has a closed-form lead time.

**Destination service.** Demand  $y_{i,t}$  is served at  $d^*$  in two ordered events within a single transition  $\xi_t \rightarrow \xi_{t+1}$ . First, scheduled arrivals at  $d^*$  are received: writing

$$A_{i,t} := \text{IT}_t[t+1, i] \quad (20)$$

for the units of item  $i$  scheduled to arrive at  $d^*$  between  $t$  and  $t+1$ , the arrivals are applied first to outstanding backlog and only the residual is added to on-hand:

$$B_{(2)}^{d^*,i} = (B_t^{d^*,i} - A_{i,t})_+, \quad \text{OH}_{(2)}^{d^*,i} = \text{OH}_t^{d^*,i} + (A_{i,t} - B_t^{d^*,i})_+. \quad (21)$$

Second, the day's demand is served from the post-arrival on-hand and any unmet portion accumulates as new backlog:

$$\text{OH}_{t+1}^{d^*,i} = (\text{OH}_{(2)}^{d^*,i} - y_{i,t})_+, \quad B_{t+1}^{d^*,i} = B_{(2)}^{d^*,i} + (y_{i,t} - \text{OH}_{(2)}^{d^*,i})_+. \quad (22)$$

The fill-rate of item  $i$  over a horizon is the ratio of served units to demanded units on that horizon.

**Standing assumptions.** Three properties are held fixed within a run:

- *Stationary topology:* the graph  $\mathcal{G}$  and the per-edge triple  $(\tau_e, V_e, K_e)$  are set at construction and not modified.
- *Fixed control policy:* the  $(s, S)$  levels, the routing rule, and the packing primitive are held constant; no online control is applied.
- *Deterministic edge transit:* edges in  $\mathcal{E}$  contribute no lead-time noise; randomness in lead times is confined to the source-level draw of (5).

### 3.2.4 Inter-warehouse flows

Cities communicate by shipping physical units across edges. This section gives the mathematical form of the three flow types that move material between cities. Each is a deterministic function of the state once the random external inputs  $(y_t, L_t)$  are fixed; the algorithmic resolution is in §3.3.1.

**Source arrivals (boundary inflow).** For  $n \in \mathcal{N}_{\text{src}}$ , source orders are placed under the  $(s, S)$  trigger of (4) and delivered after the random lead time of (5). An order placed at time unit  $t' < t$  with realized lead time  $L_{t'}^{n,i}$  delivers as a scheduled arrival at time unit  $t' + L_{t'}^{n,i}$ ; if this equals  $t$  the order arrives at  $t$  with size  $S^{n,i} - \text{OH}_{t'}^{n,i}$  (the order-up-to amount at the time of placement). The cumulative source-arrival mass between  $t$  and  $t+1$ , denoted  $A_{i,t}^{\text{src}}$ , is defined formally in (27). Source replenishment is the only mechanism that adds units to the network from outside; sources act as boundary inflow.

**Outbound dispatch (warehouses to destination).** For each item  $i$  and time unit  $t$ , the per-step target shipment volume to the destination is

$$\text{target}_{i,t} = \max\left\{0, B_t^{d^*,i} + m \tilde{\lambda}_t^i - \text{IT}_t^i - \text{OH}_t^{d^*,i}\right\}, \quad (23)$$

where  $\text{IT}_t^i = \sum_{\tau > t} \text{IT}_t[\tau, i]$  is total in-transit volume bound for  $d^*$  and  $m$  is the pipeline multiplier (a configuration parameter;  $m = 7$  in this paper). The interpretation: ship enough to cover the destination's backlog plus  $m$  time units of expected demand, minus what is already on hand or in transit. Warehouses are visited in increasing Dijkstra distance to  $d^*$ , where the edge weight on  $(u, v)$  is  $\tau_{(u,v)} / (K_{(u,v)} V_{(u,v)})$  (favoring short paths with high per-step capacity); each warehouse's contribution is bounded by its on-hand stock and by the remaining target after earlier warehouses have shipped. The flow quantity from a warehouse is the volume placed by GREEDYPACK along the resolved path; arrivals are scheduled at  $d^*$  at time unit  $t + \lceil \sum_e \tau_e \rceil$ .

**Inter-warehouse pull.** Intermediate nodes  $n \in \mathcal{N}_{\text{int}}$  trigger replenishment when  $\text{OH}_t^{n,i} < s^{n,i}$  and  $\text{Out}_t^{n,i} = \emptyset$ . The requested quantity is  $S^{n,i} - \text{OH}_t^{n,i}$ . The flow is sourced from the first upstream supplier  $u \in \mathcal{N}_{\text{int}} \cup \mathcal{N}_{\text{src}}$  with available stock  $\text{OH}_t^{u,i} > 0$ , walked in increasing total path-transit-time order. The flow quantity is the volume placed by GREEDYPACK along the path from  $u$  to  $n$ , and arrival is scheduled at  $n$  at time unit  $t + \lceil \sum_e \tau_e \rceil$ .

**Sequential coupling within a step.** In all three flow types, the actual quantity placed depends on the residual capacity of edge containers along the path, which is itself a function of earlier flows in

the same step. This makes the inter-warehouse flows sequentially coupled across items and across warehouses within the per-step update; the ordering of sub-steps in Algorithm 1 fixes this sequence. In Algorithm 1, source arrivals are realized in sub-step (vii) (order placement) and sub-step (i) (receipt), outbound dispatch in sub-step (v), and inter-warehouse pull in sub-step (vi).

### 3.3 Algorithms

This section gives the explicit algorithmic construction of the transition map  $\Psi$  defined abstractly in §3.2.1. §3.3.1 gives the seven-sub-step per-step procedure that defines  $\Psi$ . §3.3.2 defines the packing routine called from §3.3.1. §3.3.3 gives the intensity-construction procedure that produces the demand rates of §3.2.2. The parameter values used to produce the released runs are in Appendix A.

#### 3.3.1 Per-step algorithm

Algorithm 1 realizes the transition map  $\Psi$  of §3.2.1 as a sequence of seven sub-steps, executed in the fixed order given below. Each sub-step reads state written by the previous one, and the conservation identities of Proposition 4.1 hold only under this ordering.

---

**Algorithm 1** One step of the ISOMORPH simulation loop.

---

1: **Input:** time-unit index  $t$ ; graph  $\mathcal{G}$ ; per-node  $(s, S, \mu_L)$ ; current state  $\{\text{OH}, B, \text{Out}, \text{IT}\}$ ; demand function  $\text{demand}(t)$ ; smoothed demand  $\tilde{\lambda}$  with  $\alpha = 0.05$ ; pipeline multiplier  $m$ .

(1) **Receive scheduled  $(s, S)$  replenishment.**

2: **for**  $n \in \mathcal{N} \setminus \{d^*\}$  and  $i \in \mathcal{I}$  **do**  
3:     **if**  $\text{Out}^{n,i}$  is  $(\tau, q)$  with  $\tau \leq t$  **then**  
4:          $\text{OH}^{n,i} \leftarrow \text{OH}^{n,i} + q$ ; clear  $\text{Out}^{n,i}$ .  
5:     **end if**  
6: **end for**

(2) **Receive arrivals at destination; backlog cleared first.**

7: **for**  $i$  such that  $\text{IT}_t[t, i] > 0$  **do**  
8:      $q \leftarrow \text{IT}_t[t, i]$ ;  $b \leftarrow B^{d^*,i}$ .  
9:      $B^{d^*,i} \leftarrow (b - q)_+$ ;  $\text{OH}^{d^*,i} \leftarrow \text{OH}^{d^*,i} + (q - b)_+$ .  
10: **end for**

(3) **Reset edge containers each step.**

11: **for**  $e \in \mathcal{E}$  **do**  
12:      $\text{containers}_e \leftarrow [V_e] \times K_e$ .  
13: **end for**

(4) **Demand, service, and smoothed-demand update at  $d^*$ .**

14:  $y \leftarrow \text{demand}(t)$ .  
15: **for**  $i \in \mathcal{I}$  **do**  
16:      $\tilde{\lambda}_i \leftarrow \alpha y_i + (1 - \alpha) \tilde{\lambda}_i$ .  
17:      $\text{served} \leftarrow \min(\text{OH}^{d^*,i}, y_i)$ ;  $\text{unfilled} \leftarrow y_i - \text{served}$ .  
18:      $\text{OH}^{d^*,i} \leftarrow \text{OH}^{d^*,i} - \text{served}$ ;  $B^{d^*,i} \leftarrow B^{d^*,i} + \text{unfilled}$ .  
19: **end for**

(5) **Dispatch warehouses  $\rightarrow d^*$  (round-robin over items).**

20: **for**  $i$  in round-robin order **do**  
21:      $\text{target}_i \leftarrow \max\{0, B^{d^*,i} + m \tilde{\lambda}_i - \text{in-transit}_i - \text{OH}^{d^*,i}\}$ .  
22:      $\text{remaining} \leftarrow \text{target}_i$ .  
23:     **for**  $w$  in warehouses sorted by Dijkstra distance to  $d^*$  (ascending) **do**  
24:         **if**  $\text{remaining} \leq 0$  **then break**  
25:         **end if**  
26:          $q_{\text{try}} \leftarrow \min(\text{OH}^{w,i}, \text{remaining})$ .  
27:          $q_{\text{placed}} \leftarrow \text{GREEDYPACK}(i, q_{\text{try}}, \text{Path}(w, d^*))$ .  $\triangleright$  Alg. 2

```

28:     OHw,i -= qplaced; remaining -= qplaced.
29:     Schedule arrival at  $d^*$  at time unit  $t + \lceil \sum_{e \in \text{Path}(w,d^*)} \tau_e \rceil$  of size  $q_{\text{placed}}$ .
30:   end for
31: end for

```

**(6) Inter-warehouse replenishment (pull along real edges).**

```

32: for  $n \in \mathcal{N}_{\text{int}}$  in upstream-first order and each  $i \in \mathcal{I}$  do
33:   if  $\text{OH}^{n,i} < s^{n,i}$  and  $\text{Out}^{n,i}$  is empty then
34:     qty  $\leftarrow S^{n,i} - \text{OH}^{n,i}$ .
35:     for  $u$  upstream supplier of  $n$ , sorted by total transit time do
36:        $q_{\text{placed}} \leftarrow \text{GREEDYPACK}(i, \min(\text{OH}^{u,i}, \text{qty}), \text{Path}(u, n))$ .
37:       if  $q_{\text{placed}} > 0$  then
38:          $\text{OH}^{u,i} -= q_{\text{placed}}$ ;  $\text{Out}^{n,i} \leftarrow (t + \lceil \sum_e \tau_e \rceil, q_{\text{placed}})$ ; break.
39:       end if
40:     end for
41:   end if
42: end for

```

**(7) Place  $(s, S)$  orders at source nodes (random lead time).**

```

43: for  $n \in \mathcal{N}_{\text{src}}$  and  $i \in \mathcal{I}$  do
44:   if  $\text{OH}^{n,i} < s^{n,i}$  and  $\text{Out}^{n,i}$  is empty then
45:     Draw  $X \sim \mathcal{N}(\mu^{n,i}, (0.2 \mu^{n,i})^2)$ ;  $L \leftarrow \max(1, \lceil X \rceil)$ .
46:      $\text{Out}^{n,i} \leftarrow (t + L, S^{n,i} - \text{OH}^{n,i})$ .
47:   end if
48: end for

```

---

### 3.3.2 Greedy first-fit packing

The same routine handles outbound shipping (sub-step 5 of Algorithm 1) and inter-warehouse pull (sub-step 6). A call attempts to place  $Q$  units of a single item along a fixed path  $P$ , one unit at a time. For each unit, the routine walks  $P$  edge by edge and selects the first container on that edge with enough residual volume. This keeps the order of units along the path consistent with the order in which they were requested.

---

**Algorithm 2** GREEDYPACK: first-fit allocation of up to  $Q$  units of item  $i$  along a path  $P$ .

---

```

1: Input: item  $i$  with volume  $v_i$ ; max units  $Q$ ; path  $P = (e_1, \dots, e_k)$ .
2: placed  $\leftarrow 0$ .
3: for  $q = 1, \dots, Q$  do
4:   slots  $\leftarrow []$ ; ok  $\leftarrow \text{TRUE}$ .
5:   for  $e \in P$  do
6:      $j \leftarrow$  smallest index with  $\text{containers}_e[j] \geq v_i$ , or  $\perp$  if none.
7:     if  $j = \perp$  then
8:       ok  $\leftarrow \text{FALSE}$ ; break.
9:     end if
10:    Append  $(e, j)$  to slots.
11:  end for
12:  if not ok then
13:    break  $\triangleright$  stop filling; do not retry a later unit
14:  end if
15:  for  $(e, j) \in \text{slots}$  do
16:     $\text{containers}_e[j] -= v_i$ .
17:  end for
18:  placed  $\leftarrow$  placed + 1.
19: end for
20: return placed.

```

---

### 3.3.3 Intensity construction algorithm

Algorithm 3 constructs the intensity tensor  $\lambda$  used in (14). Of the five components it samples, four are drawn independently per item: yearly seasonal, weekly seasonal, AR(1) drift, and per-item burst train. The fifth,  $G(t)$ , is drawn once and reused across every item, with a per-item weight  $g_i$ . As noted in §3.2.2,  $G(t)$  is the only component that lifts every item’s intensity simultaneously, and is the mechanism by which demand forecasting and bottleneck forecasting become coupled.

---

**Algorithm 3** BUILDINTENSITY: sample the five-component intensity  $\lambda$ .

---

- 1: **Input:** item list  $\mathcal{I}$ ; horizon  $T$ ; seed.
  - 2: **Global macro-shock process**  $G(t)$ .
  - 3:  $G \leftarrow 0_T$ ; draw  $N$  uniformly from  $\{5, \dots, 11\}$ .
  - 4: **for**  $k = 1, \dots, N$  **do**
  - 5: Draw  $t_k^G$  uniform on  $\{0, \dots, T - 1\}$ ;  $\Delta_k^G$  uniform on  $\{180, \dots, 1099\}$ ;  $h_k^G \sim \mathcal{U}[0.20, 0.60]$ .
  - 6: Add trapezoidal pulse  $\pi(\cdot)$  with parameters  $(t_k^G, \Delta_k^G, h_k^G)$  to  $G$ .
  - 7: **end for**
  - 8: **Per-item components.**
  - 9: **for**  $i \in \mathcal{I}$  **do**
  - 10:  $\bar{\lambda}_i \sim \mathcal{U}[80, 250]$ .
  - 11: **Yearly:**  $S_i(t) \leftarrow a_{1,i}^{(y)} \sin(2\pi t/365 + \phi_i) + a_{2,i}^{(y)} \sin(4\pi t/365 + 0.7 \phi_i)$   
with  $a_{1,i}^{(y)} \sim \mathcal{U}[0.12, 0.28]$ ,  $a_{2,i}^{(y)} \sim \mathcal{U}[0.04, 0.10]$ ,  $\phi_i \sim \mathcal{U}[0, 2\pi]$ .
  - 12: **Weekly:**  $W_i(t) \leftarrow a_i^{(w)} \sin(2\pi(t \bmod 7)/7 + \psi_i)$  with  $a_i^{(w)} \sim \mathcal{U}[0.04, 0.10]$ ,  $\psi_i \sim \mathcal{U}[0, 2\pi]$ .
  - 13: **AR(1) drift:**  $\phi_i^{\text{AR}} \sim \mathcal{U}[0.9990, 0.9996]$ ,  $\sigma_{\text{AR},i} \sim \mathcal{U}[0.008, 0.018]$ ;  
 $A_i(0) \sim \mathcal{N}(0, 0.10^2)$ ;  $A_i(t) \leftarrow \text{clip}[\phi_i^{\text{AR}} A_i(t-1) + \mathcal{N}(0, \sigma_{\text{AR},i}^2), \pm 0.6]$ .
  - 14: **Per-item spikes**  $P_i(t)$ : burst rate  $r_i \sim \mathcal{U}[2 \cdot 10^{-4}, 10^{-3}]$ ; at each  $t$  with  $\text{Bern}(r_i) = 1$ , add a trapezoidal pulse of duration  $\mathcal{U}\{30, \dots, 179\}$  and height  $\mathcal{U}[0.20, 0.70]$ .
  - 15: **Global sensitivity:**  $g_i \sim \mathcal{U}[0.4, 1.2]$ .
  - 16: **Assemble:**  $\lambda_{i,t} \leftarrow \bar{\lambda}_i \cdot \max(0.08, 1 + S_i(t) + W_i(t) + A_i(t) + P_i(t) + g_i G(t))$ .
  - 17: **end for**
  - 18: **return**  $\lambda$ .
- 

The user configures each simulation through two kinds of parameters. *Structural parameters* are fixed within a release and define what dataset is being generated: the graph  $\mathcal{G}$ , the catalogue size  $C$ , and the time horizon  $T$ . *Scenario knobs* govern the operating regime of the network and fall into three categories: *demand structure*, *inventory*, and *edge transport*. Table 1 lists all scenario knobs with their baseline values; the complete parameter tables and their mechanisms within the simulator are detailed in Appendix A.

## 4 The right state space and its consequences

Unlike existing resources that track only per-node demand or inventory [Wasi et al., 2024, Naik et al., 2025], the state vector  $\xi_t$  in ISOMORPH carries outstanding orders, scheduled arrivals, and smoothed demand estimates alongside per-node inventory. These auxiliary components lift the system into a space where three properties emerge: the dynamics are Markovian (§4.1), three discrete conservation laws hold exactly on every sample path (§4.2), and the discrete laws align with classical continuum transport and queueing equations (§4.3).

### 4.1 Markov property

Without the auxiliary components  $\text{Out}_t$ ,  $\text{IT}_t$ , and  $\tilde{\lambda}_t$  in the state, the next-step inventory would depend on a window of past dispatches and lead-time draws, not on  $\xi_t$  alone: the dynamics would require history and the Markov property would fail. By including them, the system closes into a Markov chain  $\xi_{t+1} = \Psi(\xi_t, y_t, L_t)$  whose transition probability acts linearly on the empirical

Table 1: Scenario knobs of ISOMORPH with baseline values; full distributions in Appendix A.

Symbol	Description	Baseline
<i>Demand structure</i>		
$\bar{\lambda}_i$	per-item base demand intensity	$\mathcal{U}[80, 250]$
$a_i^{(y)}, a_i^{(w)}$	yearly and weekly seasonal amplitudes	$a^{(y)} \in [0.04, 0.28], a^{(w)} \in [0.04, 0.10]$
$\phi_i^{\text{AR}}$	AR(1) drift coefficient	$\mathcal{U}[0.9990, 0.9996]$
$\sigma_{\text{AR},i}$	AR(1) innovation scale	$\mathcal{U}[0.008, 0.018]$
$r_i$	per-item burst rate	$\mathcal{U}[2 \cdot 10^{-4}, 10^{-3}]$
$h_{i,k}^P$	per-item burst height	$\mathcal{U}[0.20, 0.70]$
$N$	number of macro-shock events	$\mathcal{U}\{5, \dots, 11\}$
$h_k^G$	per-event macro-shock height	$\mathcal{U}[0.20, 0.60]$
<i>Inventory</i>		
$(s_n, S_n)$	per-node $(s, S)$ reorder threshold and target	node-specific
$\mu^n$	mean lead time at source node $n$	3 time units
<i>Edge transport</i>		
$K_e$	per-step container count on edge $e$	3 on every edge
$\rho$	target load factor in last-mile back-solve	1.20
$m$	proactive-shipping pipeline multiplier	7

distribution of the state (§3.2.1)—the right space for scalable simulation, forward UQ, and downstream stochastic control.

## 4.2 Discrete conservation laws

The same state completeness that enables the Markov property also reveals conservation structure structurally encoded in the transition function  $\Psi$ . The network-internal stock  $I_{i,t}$  in (26) sums over on-hand, in-transit, and scheduled-arrival components—all present in  $\xi_t$  by design—so the conservation laws below are expressible as closed-form functions of the current state.

**Proposition 4.1** (Conservation of units and demand events). *For each item  $i \in \mathcal{I}$  and time unit  $t \in \{0, \dots, T-1\}$ , let  $u_{i,t}^e$  denote the units of item  $i$  placed onto edge  $e$  at sub-steps (5)–(6) of Algorithm 1. Define per-node receipts and dispatches in  $[t, t+1]$  as*

$$R_t^{n,i} := \begin{cases} q, & n \neq d^* \text{ and } \text{Out}_t^{n,i} = (t+1, q), \\ (A_{i,t} - B_t^{d^*,i})_+, & n = d^*, \\ 0, & \text{otherwise;} \end{cases} \quad (24)$$

$$D_t^{n,i} := \begin{cases} \sum_{(n,v) \in \mathcal{E}} u_{i,t}^{(n,v)}, & n \neq d^*, \\ \min(\text{OH}_{(2)}^{d^*,i}, y_{i,t}), & n = d^*. \end{cases} \quad (25)$$

Define the network-internal stock

$$I_{i,t} := \sum_{n \in \mathcal{N}} \text{OH}_t^{n,i} + \sum_{(u,v) \in \mathcal{E}, v \neq d^*} q_{i,t}^{u \rightarrow v} + \sum_{\tau > t} \text{IT}_t[\tau, i], \quad (26)$$

where  $q_{i,t}^{u \rightarrow v}$  is the per-edge in-transit count defined in §3.2.1 and  $\text{IT}_t[\tau, i]$  is the multiplicity of arrivals scheduled at  $d^*$  at time unit  $\tau$  for item  $i$ . Define the source arrivals between  $t$  and  $t+1$  as

$$A_{i,t}^{\text{src}} := \sum_{n \in \mathcal{N}_{\text{src}}} \mathbf{1}\{\text{Out}_t^{n,i} = (\tau, q), \tau = t+1\} \cdot q, \quad (27)$$

the mass arriving at non-destination nodes from sources between time units  $t$  and  $t+1$ . With  $A_{i,t} := \text{IT}_t[t+1, i]$  and  $\text{OH}_{(2)}^{d^*,i} = \text{OH}_t^{d^*,i} + (A_{i,t} - B_t^{d^*,i})_+$  as defined in (20)–(21), define the total destination outflow as the sum of the arrival-clears-backlog flow and the immediate-service flow:

$$S_{i,t} := \min(A_{i,t}, B_t^{d^*,i}) + \min(\text{OH}_{(2)}^{d^*,i}, y_{i,t}). \quad (28)$$

Then the chain  $(\xi_t)_{t \geq 0}$  satisfies, almost surely for all  $t \in \{0, \dots, T-2\}$  and  $i \in \mathcal{I}$ :

$$(a) \text{ Per-node mass conservation: } \quad \text{OH}_{t+1}^{n,i} = \text{OH}_t^{n,i} + R_t^{n,i} - D_t^{n,i}, \quad \forall n \in \mathcal{N}, \quad (29)$$

$$(b) \text{ Global mass conservation: } \quad I_{i,t+1} = I_{i,t} + A_{i,t}^{\text{src}} - S_{i,t}, \quad (30)$$

$$(c) \text{ Backlog conservation: } \quad B_{t+1}^{d^*,i} = B_t^{d^*,i} + (y_{i,t} - \text{OH}_t^{d^*,i})_+. \quad (31)$$

*Proof. Part (a).* Fix  $n \in \mathcal{N}$  and  $i \in \mathcal{I}$ . We trace changes to  $\text{OH}^{n,i}$  across the seven sub-steps of Algorithm 1 during the transition from  $t$  to  $t+1$ .

*Case  $n \neq d^*$ .* Sub-step (1) increments  $\text{OH}^{n,i}$  by  $q$  when  $\text{Out}_t^{n,i} = (t+1, q)$ , and by zero otherwise; this matches  $R_t^{n,i}$  as defined in (24). Sub-steps (2) and (4) act only at  $d^*$  and leave  $\text{OH}^{n,i}$  unchanged. Sub-step (3) resets edge containers without modifying any node's on-hand. Sub-steps (5) and (6) decrement  $\text{OH}^{n,i}$  by exactly the units placed onto  $n$ 's outgoing edges via GREEDYPACK, i.e.,  $\sum_{(n,v) \in \mathcal{E}} u_{i,t}^{(n,v)} = D_t^{n,i}$ . Sub-step (7) modifies  $\text{Out}^{n,i}$  for  $n \in \mathcal{N}_{\text{src}}$  but does not modify  $\text{OH}^{n,i}$ . Collecting:  $\text{OH}_{t+1}^{n,i} = \text{OH}_t^{n,i} + R_t^{n,i} - D_t^{n,i}$ .

*Case  $n = d^*$ .* Sub-step (1) acts only at non-destination nodes. Sub-step (2) increments  $\text{OH}^{d^*,i}$  by  $(A_{i,t} - B_t^{d^*,i})_+ = R_t^{d^*,i}$  (the post-backlog residual of arriving units, per (21)). Sub-step (3) resets edge containers. Sub-step (4) decrements  $\text{OH}^{d^*,i}$  by  $\min(\text{OH}_{(2)}^{d^*,i}, y_{i,t}) = D_t^{d^*,i}$  (the served quantity, second term of  $S_{i,t}$  in (28)). Sub-steps (5)–(7) do not modify  $\text{OH}^{d^*,i}$ : the destination is excluded from the warehouse loop in (5), is not an upstream supplier in (6), and is not a source in (7). Hence  $\text{OH}_{t+1}^{d^*,i} = \text{OH}_t^{d^*,i} + R_t^{d^*,i} - D_t^{d^*,i}$ .

**Part (b).** Summing Part (a) over all nodes and adding the in-transit and scheduled-arrival components: routing along edges transfers units between  $\sum_n \text{OH}^{n,i}$  and  $\sum_e q_i^{u \rightarrow v}$  without changing the total  $I_{i,t}$  defined in (26). The only mechanisms that change  $I_{i,t}$  are source arrivals (sub-steps i and vii), which add  $A_{i,t}^{\text{src}}$ , and destination service (sub-steps ii and iv), which removes  $S_{i,t}$ . Therefore  $I_{i,t+1} - I_{i,t} = A_{i,t}^{\text{src}} - S_{i,t}$  almost surely.

**Part (c).** Immediate from (21)–(22) of §3.2.3: at sub-step (ii), backlog is updated to  $B_{(2)}^{d^*,i} = (B_t^{d^*,i} - A_{i,t})_+$ ; at sub-step (iv), the unfilled remainder  $(y_{i,t} - \text{OH}_{(2)}^{d^*,i})_+$  is added to  $B_{(2)}^{d^*,i}$  to give  $B_{t+1}^{d^*,i}$ . No other sub-step modifies  $B^{d^*,i}$ .  $\square$

All three identities are preserved exactly—not approximately—because the simulator's transitions are bookkeeping operations on integer counts, with no rounding or stochastic loss inside the network. Any deviation at any  $(t, i)$  in a released run would indicate a bug in the simulator, corruption in the released files, or a mismatch between the model and its algorithmic realization.

**Conservation laws as structural invariants of the DBN.** All three laws hold pathwise—for every realization of the random external inputs  $(y_t, L_t)$ , not only in expectation. The two boundary terms of the global mass conservation align with the two random input nodes in the Markov chain (Figure 1):  $A_{i,t}^{\text{src}}$  is determined by the lead-time vector  $L_t$  (which controls when source orders arrive), and the service component of  $S_{i,t}$  is determined by the demand vector  $y_t$  together with the on-hand state at  $d^*$ . The places where randomness enters the chain are the same places where mass crosses the boundary of the conserved domain. Internal flows (routing, packing, inter-warehouse transfers) are deterministic given  $(y_t, L_t)$  and conservative by construction. The conservation laws are therefore structural invariants of the Markov chain: they constrain every sample path the simulator can produce.

### 4.3 Continuous-time fluid limit: coupled transport and queuing

This section highlights the mathematical structure of ISOMORPH and connects it to the literature on queuing systems and their fluid limits. First, the three discrete conservation laws of Proposition 4.1 are not isolated bookkeeping identities: they are the pre-limit forms of classical continuum equations that govern the fluid limit of the Markov chain. Consider a sequence of systems indexed by a system-size parameter  $N$ , in which the catalogue size, demand intensities, edge capacities, and control thresholds  $(s, S)$  are all scaled by  $N$  simultaneously. Under this Kurtz-type law-of-large-numbers

scaling [Kurtz, 1970], each individual unit becomes a vanishing fraction of the total, and the rescaled density  $\rho^{N,n,i}(t) = N^{-1}\text{OH}_{[tN]}^{n,i}$  converges in probability to the deterministic solution of a coupled system: a transport equation on the graph  $\mathcal{G}$  governing inventory, and a Skorokhod-reflected ODE at  $d^*$  governing backlog. The discrete conservation laws hold at every finite  $N$  and pass to the limit, making the continuum system their deterministic counterpart.

At the discrete level, the simulator is a jump process on a network of control volumes: each node  $n \in \mathcal{N}$  is a fixed control volume that accumulates on-hand inventory  $\text{OH}_t^{n,i}$ , and the edges  $\mathcal{E}$  are conduits that carry discrete unit-valued jumps between control volumes. The fluid limit smooths these integer-valued jumps into continuous densities and fluxes.

**Transport (inventory side).** In the fluid limit, the per-node, per-item inventory satisfies a delay-differential equation on  $\mathcal{G}$ : for each node  $n \in \mathcal{N}$  and item  $i \in \mathcal{I}$ ,

$$\partial_t \rho^{n,i}(t) = \sum_{u:(u,n) \in \mathcal{E}} \phi_i^{u \rightarrow n}(t - \tau_{u,n}) - \sum_{v:(n,v) \in \mathcal{E}} \phi_i^{n \rightarrow v}(t) + r_i^n(t) \mathbf{1}\{n \in \mathcal{N}_{\text{src}}\} - s_i^n(t) \mathbf{1}\{n = d^*\}, \quad (32)$$

subject to edge capacity constraints  $\sum_i v_i \phi_i^{u \rightarrow v}(t) \leq \kappa_{u,v}$ . This is the continuous form of the local continuity equation  $\partial_t \rho + \nabla \cdot j = \sigma$  on the graph, where the delayed inflows from upstream edges play the role of flux divergence, and source replenishment  $r_i^n$  and destination service  $s_i^n$  act as boundary source/sink terms.

The per-node mass conservation (29) is the time-discretized form of (32): on-hand inventory  $\text{OH}_t^{n,i}$  is the local density in the control volume at node  $n$ , receipts  $R_t^{n,i}$  and dispatches  $D_t^{n,i}$  are the discrete inflow and outflow across the control-volume boundary, and their difference is the discrete divergence. Integrating over the entire graph—summing over all control volumes—yields the global mass conservation (30): internal fluxes cancel in pairs, and only boundary terms survive, giving the discrete analog of  $\frac{d}{dt} \int_{\Omega} \rho = - \int_{\partial\Omega} j \cdot n + \int_{\Omega} \sigma$ .

**Queueing (demand side).** In classical queueing theory, the queue length  $Q$  evolves according to the fluid model  $dQ/dt = \lambda(t) - \mu(t)$ , where  $\lambda$  is the arrival rate and  $\mu$  is the service rate, subject to the constraint  $Q \geq 0$  (Skorokhod reflection). In ISOMORPH, the backlog  $B_t^{d^*,i}$  at the destination  $d^*$  for each item  $i \in \mathcal{I}$  plays the role of  $Q$ , demand  $y_{i,t}$  plays the role of  $\lambda$ , and fulfilled orders  $\min(\text{OH}_t^{d^*,i}, y_{i,t})$  play the role of  $\mu$ . The discrete backlog conservation (31) is the time-discretized form of this fluid model, with the  $(\cdot)_+$  operator enforcing non-negativity.

In the fluid limit, the rescaled backlog at the destination  $d^*$  for each item  $i \in \mathcal{I}$  converges to the Skorokhod-reflected ODE

$$\partial_t b^{d^*,i} = (\lambda_i - \rho^{d^*,i})_+ - (A_i - b^{d^*,i})_+, \quad (33)$$

where the first term adds unmet demand (arrivals exceeding on-hand density) and the second term drains backlog when shipments arrive at  $d^*$ .

**Coupling at the destination.** The transport and queueing subsystems couple at  $d^*$ : the service term  $S_{i,t}$  is simultaneously the boundary outflow of the transport equation (32) and the service rate of the queue (33). The transport network's ability to deliver units to  $d^*$  determines the queue's service rate, and the queue's backlog state feeds back into dispatch targets through the proactive shipping formula of sub-step (5). This coupling persists in both the discrete and continuum settings. Table 2 summarizes the full correspondence.

Each sub-step of Algorithm 1 contributes a jump of size  $O(1/N)$  at rate  $O(N)$  to the rescaled generator, placing the chain in the regime where Kurtz's theorem [Kurtz, 1970] applies. The  $(s, S)$  replenishment policy introduces switching boundaries at the reorder threshold, producing either a hybrid system with Filippov solutions or, under a smoothed base-stock control, a classical ODE; both are standard in the fluid-network literature [Chen and Yao, 2001, Mandelbaum and Pats, 1998]. The edge capacity constraints produce a complementarity structure—flow at capacity implies zero slack at the controller—shared with fluid models of multi-class queueing networks [Whitt, 2002]. A rigorous formulation of the limit theorem and the associated diffusion correction (CLT-type Brownian fluctuations around  $\rho$ ) is of independent mathematical, computational and statistical interest.

Table 2: Correspondence between the fluid-limit equations and the discrete conservation laws of Proposition 4.1. Each node  $n \in \mathcal{N}$  serves as a control volume; edges carry discrete unit-valued jumps that become continuous fluxes in the fluid limit.

Fluid limit	Discrete (ISOMORPH)
<i>(a) Per-node mass conservation (29): local continuity equation (32)</i>	
density $\rho^{n,i}(t)$	on-hand inventory $\text{OH}_t^{n,i}$
flux $\phi_i^{u \rightarrow v}$	shipment flow $u_{i,t}^e$ along edge $e$
divergence	net outflow from control volume at node $n$ : $D_t^{n,i} - R_t^{n,i}$ (Eqs. 25, 24)
source/sink $r_i^n, s_i^n$	$A_{i,t}^{\text{src}}$ (27) (source inflow), $S_{i,t}$ (28) (destination outflow)
<i>(b) Global mass conservation (30): integrated form</i>	
integrated density $\int_{\Omega} \rho$	network-internal stock $I_{i,t}$ (26)
boundary flux $\int_{\partial\Omega} j \cdot n$	$A_{i,t}^{\text{src}}$ (27) (in), $S_{i,t}$ (28) (out)
<i>(c) Backlog conservation (31): reflected ODE (33)</i>	
queue length $b^{d^*,i}$	backlog $B_t^{d^*,i}$
arrival rate $\lambda_i$	demand $y_{i,t}$
service rate	$\min(\text{OH}_t^{d^*,i}, y_{i,t})$
<i>Coupling at <math>d^*</math>: <math>S_{i,t} = \text{transport outflow} = \text{queue service rate}</math></i>	

## 5 Released datasets

We describe the user input configurations and output sequences for the released datasets in two cardinality regimes ( $C=50$  and  $C=200$ ) in §5.1. In §5.2, we validate the datasets by confirming that a well-known domain-specific phenomenon—the bullwhip effect—emerges at empirically consistent magnitudes, and present two conservation laws for verifying sequence fidelity when users modify the simulator.

### 5.1 User input configurations and output sequences

The released datasets are configured through the structural parameters and scenario knobs of §3.

**Structural parameters.** All releases in this paper use the following configuration:

- *Graph*: the 13-node U.S. network of Figure 1(a)—three sources {San Francisco, St. Louis, Orlando}, nine intermediate warehouses organized in five tiers (hub, three mid-level tiers, and last-mile), and destination New York. All three sources converge at Nashville and fan out through Atlanta; every shipment to New York passes through one of two last-mile edges (Philadelphia→New York or Baltimore→New York).
- *Cardinality*: two regimes,  $C=50$  and  $C=200$ . The two regimes share the same demand parameters, reorder thresholds ( $s, S$ ), routing, and packing rules; only the edge capacities differ. Upstream edge container volumes scale linearly with  $C$ , so they are four times larger at  $C=200$  when the per-step container count  $K_e$  is held fixed. The two last-mile edges are sized by back-solving the realized mean intensity (§A.4). The first 50 items at  $C=200$  coincide with the entire  $C=50$  release under the same seed, so  $C=50$  is suitable for faster model development with fewer item channels while  $C=200$  tests scalability to a larger catalogue.
- *Horizon*:  $T=52,560$  time units.

**Scenario knobs.** We construct six one-at-a-time sweeps—three perturbing the demand process and three perturbing the network’s response—each across five settings (a shared baseline plus four perturbations), producing  $6 \times 5 = 30$  rollouts on the  $C=50$  regime (sweep definitions in Table 13, App. B.4); the  $C=200$  regime uses baseline settings only. Their use for forward UQ is discussed in §6.2.

Each rollout produces a complete record of the network’s state and activity at every step.

**Output sequences.** Each rollout records the full network state trajectory: per-item demand, service, and backlog at the destination; per-node inventory levels; in-transit volumes; and per-edge shipments

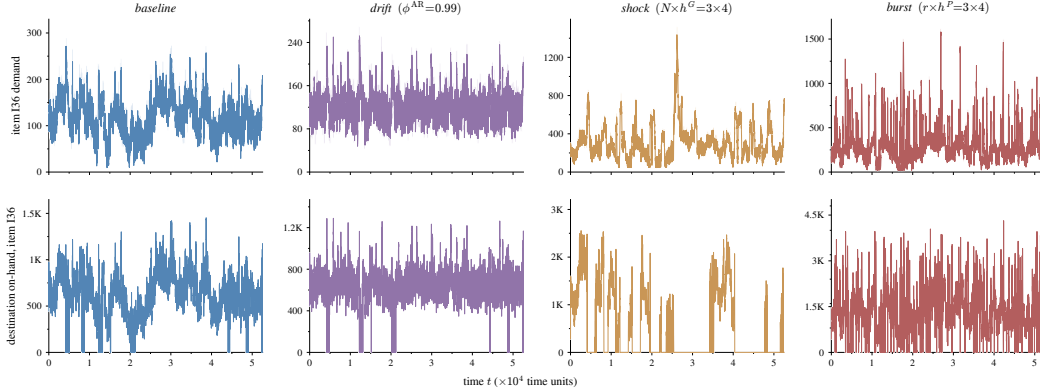


Figure 4: Diversity of dynamics generated by the simulator for a single item (I36) across four scenarios. **Top row:** per-item demand series. **Bottom row:** destination on-hand stock for the same item. Each column is a different scenario: baseline, drift ( $\phi^{\text{AR}}=0.99$ ), shock ( $N \times h^G=3 \times 4$ ), and burst ( $r \times h^P=3 \times 4$ ). Drift compresses the demand range and depletes stock more persistently; shock introduces large global surges that periodically drive stock to zero; burst produces sharp per-item spikes with corresponding stock crashes. Time on the  $x$ -axis is in units of  $10^4$  time steps (full horizon  $T = 52,560$ ).

with resolved paths. Per-file schemas are in Appendix B. In the TSF evaluation of §6, we forecast the per-item demand series from `daily_records.csv`; Figure 6 (App. B) shows sample channels from the  $C=50$  baseline and their interactions during a demand spike. Diverse dynamics emerge from different scenario configurations (scenario definitions in Table 13, App. B.4; instantiation in §6.2); Figure 4 illustrates this for a single item across four scenarios and two output variables.

**Alignment with TSF benchmarks.** The output sequences are structured to be directly usable as time-series forecasting benchmark datasets in the same sense as ETT, Weather, or Electricity, supporting both univariate and multivariate evaluation across multiple prediction horizons at fixed frequency. The released datasets can serve as standalone benchmarks or as a new logistics domain entry in multi-domain suites such as GIFT-Eval [Aksu et al., 2024]. Moreover, the simulator is fully open-source and modular, so users can generate data at different scales (e.g. catalogue size or graph structure), parameter settings, control rules, and time resolutions tailored to their own setting.

## 5.2 Validation

We validate the released data by checking whether it exhibits the *bullwhip effect*, the standard empirical signature of supply-chain dynamics in which demand variability amplifies as one moves upstream from the customer-facing destination toward the factories. Cachon et al. [2007] measured this across 74 U.S. industries and found that amplification is real but varies across industries and is not always monotonic along the chain. We compute the same amplification ratio at every non-source node (Table 3; method in App. D.1). All six tier-level monthly  $\bar{B}$  values fall in  $[1.07, 1.57]$ , inside the  $[0.97, 1.90]$  range spanning the 50th–90th percentiles of the empirical distribution. Amplification is non-monotonic across tiers, peaking at the last-mile nodes ( $\bar{B} = 1.57$ ), consistent with the empirical findings. Per-node values are in Table 19 (App. D.2).

The simulator also satisfies three conservation laws (Proposition 4.1, §4.2) that are structurally encoded in the Markov transition function  $\Psi$  by the right state space design of §4. Because every unit and every demand event is accounted for at every step, downstream metrics—fill rate, service level, backlog counts—are well-defined and recoverable from the released data. When users add their own control rules to the simulator, these conservation laws, or adapted versions of them, can verify the fidelity of the modified implementation.

Table 3: Bullwhip amplification by tier on the  $C=50$  release.  $\bar{B} = \text{Var}(\text{inflow}) / \text{Var}(\text{outflow})$ , computed per (node, item) and averaged over items, then over nodes in each tier. The three source nodes are excluded because they have no inflow on the released edges. The “Daily” column is inflated near the destination because shipments arrive in bursts within a month; the “Monthly” column smooths this out and is the granularity comparable to Cachon et al. [2007]’s industry-level evidence.

Tier	Nodes	Daily $\bar{B}$	Monthly $\bar{B}$
Destination	New York	9.03	1.43
Tier-5 (LM)	Baltimore, Philadelphia	13.00	1.57
Tier-4	Columbus, Richmond	1.40	1.30
Tier-3	Charlotte, Chicago, Memphis	1.16	1.24
Tier-2	Atlanta	1.29	1.16
Hub	Nashville	0.97	1.07

## 6 Digital Twin meets TSF foundation models

Pairing a digital twin with TSF foundation models unlocks several capabilities: datasets generated by the simulator introduce the logistics domain to existing TSF benchmarks (§6.1); foundation models can serve as fast surrogates for forward UQ over parameter and model uncertainty; and this allows the foundation models to be evaluated on their ability to generalize under perturbations in the dynamics’ parameters (§6.2). Experiments probing these capabilities are in §6.3.

### 6.1 TSF benchmarking for logistics

ISOMORPH introduces the logistics domain to TSF benchmarking. Different scenario configurations produce diverse sequential patterns—oscillatory reorder cycles, persistent drift, global shocks, and localized bursts (Figure 4)—that are largely absent from existing benchmark collections. To test whether these patterns pose new challenges, we evaluate pretrained foundation models on our datasets and compare with reference values from standard benchmarks (Table 4).

We choose four models to cover the main architectural choices in TSF foundation models: **Chronos-T5** [Ansari et al., 2024] (tokenized values, encoder-decoder T5 backbone, real+KernelSynth pretraining); **Moirai-1.1-R** [Woo et al., 2024] (masked encoder, pretrained on LOTSA); **TimesFM-2.0** [Das et al., 2023] (decoder-only, trained on Google Trends and Wikipedia pageviews); and **Lag-Llama** [Rasul et al., 2023] (decoder-only with explicit lag features, multi-domain corpus).

All four models see  $L=512$  past steps and predict at horizons  $h \in \{1, 7, 14, 30\}$ , which fall within the short-to-medium range of GIFT-Eval’s 97 task configurations ( $h \in [6, 900]$ ) [Aksu et al., 2024]. The forecast window slides across the test split (the final 15% of each release) in non-overlapping steps of 30, giving  $|W|=262$  windows per release. The forecast target is the per-item demand  $y_{i,t}$ .

We report Mean Absolute Scaled Error (MASE) following the GIFT-Eval formula [Aksu et al., 2024]: at each item and horizon, the model’s mean absolute error is divided by that of a seasonal-naive baseline  $\hat{y}_{t+k}^{\text{SN}} = y_{t+k-7}$ , and the per-item ratios are combined as a geometric mean (formal definition in App. C.1). MASE provides standard reference values that have been fully tested across existing benchmarks, enabling direct comparison of our dataset’s difficulty against established collections.

### 6.2 Zero-shot forward UQ from the digital twin and foundation models

Standard fixed datasets limit UQ to aleatoric uncertainty—synthetic perturbations such as additive noise, masking, or jitter. Because ISOMORPH exposes the full data-generating process, we can quantify the effect of two additional sources of uncertainty on the foundation models’ predictions. *Parameter uncertainty* varies the numerical values of scenario knobs (Table 1) while keeping the model structure fixed; *model uncertainty* substitutes structural choices—such as the Poisson demand family (Eq. 14, §3.2.2), rectangular pulse shapes for shocks and bursts (Eqs. 19–18), or the  $(s, S)$  replenishment policy (§3.2.3)—while keeping knob values fixed. In both cases, the simulator generates a new rollout for each configuration, and the pretrained foundation model is applied zero-shot, allowing us to attribute prediction variability directly to the input perturbations and produce confidence bands from multiple configurations.

Table 4: MASE on the  $C=50$  datasets for four TSF foundation models at four prediction horizons  $h$  (context length  $L = 512$ ). Baseline values are shown first, with the average MASE across five demand-side scenarios in parentheses (per-scenario breakdown in Table 16, App. C). The Ref. column provides each model’s aggregate MASE from the public GIFT-Eval leaderboard for comparison. Our prediction horizons ( $h \leq 30$ ) fall within the short-to-medium range of GIFT-Eval’s configurations ( $h \in [6, 900]$ ). Bold entries exceed the model’s own reference value, suggesting increasing difficulty at longer horizons on this domain.

Model	$h=1$	$h=7$	$h=14$	$h=30$	Ref.
Chronos	0.769 (0.718)	0.818 (0.801)	0.874 ( <b>0.913</b> )	<b>1.007 (1.183)</b>	0.876
Moirai	0.786 (0.745)	0.831 (0.826)	0.889 ( <b>0.933</b> )	<b>1.028 (1.183)</b>	0.901
TimesFM	0.742 (0.699)	<b>0.786 (0.783)</b>	<b>0.843 (0.895)</b>	<b>0.978 (1.149)</b>	0.758
Lag-Llama	1.027 (1.062)	<b>1.292 (1.521)</b>	<b>1.396 (1.719)</b>	<b>1.601 (2.033)</b>	1.228

We perform forward UQ with respect to parameter uncertainty by drawing  $K=20$  configurations via Latin-hypercube sampling over three demand-side knobs: burst height  $h^P \in [0.5, 2.0]$ , macro-shock height  $h^G \in [0.5, 2.0]$ , and AR(1) drift coefficient  $\phi^{\text{AR}} \in [0.95, 0.999]$ , generating one rollout per configuration with all three knobs varying jointly. Both the digital twin and the foundation models produce forecast envelopes (confidence bands) over the prediction window; Figure 5 shows the resulting envelopes for item I01’s demand series.

### 6.3 Results

**TSF performance: baseline and scenario average.** Table 4 reports MASE for all four models on the  $C=50$  baseline and averaged across five perturbed scenarios defined in B.4 at four horizons ( $C=200$  baseline in Table 14, App. C; per-scenario breakdown in Table 16, App. C). At short horizons ( $h \leq 7$ ), all models score below their GIFT-Eval reference values, as expected: in a short prediction window, domain-specific patterns have limited opportunity to manifest. As the horizon grows ( $h \geq 14$  and especially  $h = 30$ ), prediction errors rise beyond the reference values—even though our horizons remain in the short-to-medium range of GIFT-Eval’s configurations ( $h \in [6, 900]$ )—and the gap widens further under perturbed scenarios. This suggests that the logistics-domain dynamics in our data become increasingly challenging at longer horizons, pointing to potential gains from fine-tuning and incorporation of ISOMORPH into benchmark datasets such as GIFT-Eval as a new logistics domain.

**Zero-shot forward UQ.** Figure 5 shows forecast envelopes (confidence bands) from the digital twin and four foundation models. the foundation models’ forecast envelopes cover similar regions to the digital twin’s forecast envelope across all four models and all prediction horizons, and the median forecasts track the digital twin’s median closely. This demonstrates that zero-shot foundation models can serve as effective proxies for propagating parameter uncertainty through the simulator without retraining. Compared to the  $K$  simulator runs, foundation model inference in the zero-shot setting adds negligible cost, following the spirit of neural-network-surrogate UQ [Taverniers et al., 2021]. Additional forecast windows in Figure 7 (App. D.3) show consistent behavior.

## 7 Limitations and scope of claims

**Scope of simulator.** The released datasets use a fixed set of structural parameters—a single 13-node U.S. network, two catalogue sizes, and one time horizon—with variation limited to the scenario knobs of Table 1. The simulator is open-source and accepts arbitrary user-supplied graphs, so extending to larger or differently structured networks is straightforward. All releases share the same transition rules:  $(s, S)$  replenishment, Dijkstra routing, and greedy first-fit packing (Algorithm 1). The modular codebase allows each of these to be replaced independently, and the conservation laws of Proposition 4.1 (or adapted versions) can verify fidelity of any modified implementation.

**Scope of evaluation.** We evaluate the four foundation models on ISOMORPH releases only; a side-by-side comparison on a real logistics dataset is not included, as proprietary access restrictions make such data difficult to obtain. The evaluation targets the per-item demand series  $y_{i,t}$  exclusively.

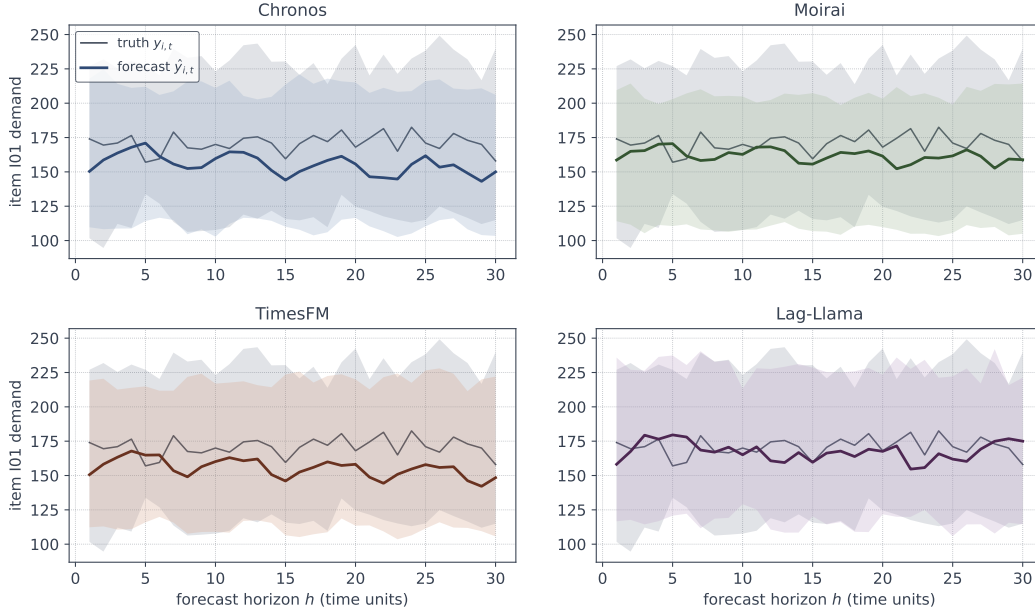


Figure 5: Forward UQ forecast envelope for item I01 at one forecast window. Each panel shows a different foundation model. The shaded band spans the  $K=20$  Latin-hypercube rollouts over three demand-side scenario knobs:  $h^P \in [0.5, 2.0]$ ,  $h^G \in [0.5, 2.0]$ , and  $\phi^{\text{AR}} \in [0.95, 0.999]$ . The colored line is the median forecast and the dark gray line is the median of the digital twin’s envelope. The light gray shaded region is the digital twin’s forecast envelope, and the light colored shaded region is the foundation model’s forecast envelope.

Extending the forecast targets to wider network state variables—such as edge utilization, fill rate, or backlog—requires the user to design the appropriate problem formulation.

## 8 Release and maintenance

The simulator code, evaluation pipeline, and data loaders are released under MIT at <https://github.com/tuhinsahai/ISOMORPH>; the datasets used in this work are available from the authors upon request. Bug reports and feature requests use the repository’s issue tracker; the corresponding author will respond to issues for at least two years after publication.

## 9 Conclusion and outlook

We presented ISOMORPH, an open-source digital twin of a multi-echelon logistics network whose every parameter is physically interpretable and user-configurable. By augmenting per-node on-hand inventory with outstanding orders, in-transit shipments, and a smoothed demand estimate, the simulator closes the dynamics as a Markov chain on a high-dimensional but tractable state space, with a deterministic transition function driven by two random inputs. The chain satisfies pathwise conservation laws that can serve as verification tools when users modify the codebase. We released datasets at two cardinalities ( $C=50$  and  $C=200$ ) together with 30 scenario rollouts and 20 Latin-hypercube perturbations for forward UQ, validated by reproducing the bullwhip effect at empirically consistent magnitudes.

Pairing the digital twin with four TSF foundation models demonstrates two capabilities. First, the released datasets introduce the logistics domain to TSF benchmarking: zero-shot MASE values exceed public GIFT-Eval references at moderate prediction horizons ( $h \geq 14$ ), suggesting that logistics-domain dynamics pose challenges not covered by current benchmark collections. Second, propagating parameter uncertainty through the simulator yields forecast envelopes that all four models

capture well in the zero-shot setting, demonstrating that pretrained foundation models can serve as effective proxies for forward UQ without retraining.

**Outlook.** Several directions can extend the present work. On the simulator side, richer shock models (correlated multi-region events, targeted supplier failures), additional per-node covariates (weather, labor events), and alternative control policies would broaden the range of generatable dynamics. On the evaluation side, extending forecast targets to network state variables (edge utilization, fill rate, backlog), adopting probabilistic metrics (CRPS, quantile loss), and instantiating model uncertainty through structural substitutions in the simulator are natural next steps. Two application directions follow from the pairing: fine-tuning a foundation model on ISOMORPH-generated data to produce a logistics-domain surrogate, and submitting ISOMORPH datasets to GIFT-Eval [Aksu et al., 2024] as a new logistics domain entry. Finally, the three conservation laws impose algebraic relations across demand, service, and backlog channels that reflect the coupled transport-queueing structure of the simulator. Structure-aware TSF architectures could be trained to respect these constraints, connecting to established directions in physics-informed forecasting [Beucler et al., 2021, Naik et al., 2025] and fluid-limit theory for jump processes [Kurtz, 1970, Chen and Yao, 2001].

## References

- Taha Aksu, Gerald Woo, Juncheng Liu, Xu Liu, Chenghao Liu, Silvio Savarese, Caiming Xiong, and Doyen Sahoo. GIFT-eval: A benchmark for general time series forecasting model evaluation. In *NeurIPS Workshop on Time Series in the Age of Large Models*, 2024. URL <https://openreview.net/forum?id=Z2cMO0ANFX>.
- Abdul Fatir Ansari, Lorenzo Stella, Ali Caner Turkmen, Xiyuan Zhang, Pedro Mercado, Huibin Shen, Oleksandr Shchur, Syama Sundar Rangapuram, Sebastian Pineda Arango, Shubham Kapoor, Jasper Zschiegner, Danielle C. Maddix, Hao Wang, Michael W. Mahoney, Kari Torkkola, Andrew Gordon Wilson, Michael Bohlke-Schneider, and Bernie Wang. Chronos: Learning the language of time series. *Transactions on Machine Learning Research*, 2024. ISSN 2835-8856. URL <https://openreview.net/forum?id=gerNCVqqtR>. Expert Certification.
- Mansur Arief. Deepbullwhip: An open-source simulation and benchmarking for multi-echelon bullwhip analyses. 04 2026. doi: 10.48550/arXiv.2604.13478.
- Tom Beucler, Michael Pritchard, Stephan Rasp, Jordan Ott, Pierre Baldi, and Pierre Gentine. Enforcing analytic constraints in neural networks emulating physical systems. *Physical Review Letters*, 126(9):098302, 2021. doi: 10.1103/PhysRevLett.126.098302.
- G rard Cachon, Taylor Randall, and Glen Schmidt. In search of the bullwhip effect. *Manufacturing & Service Operations Management*, 9:457–479, 10 2007. doi: 10.1287/msom.1060.0149.
- Hong Chen and David D. Yao. *Fundamentals of Queueing Networks: Performance, Asymptotics, and Optimization*. Stochastic Modelling and Applied Probability. Springer, 2001.
- Abhimanyu Das, Weihao Kong, Rajat Sen, and Yichen Zhou. A decoder-only foundation model for time-series forecasting. In *International Conference on Machine Learning*, 2023. URL <https://api.semanticscholar.org/CorpusID:264172792>.
- Samuel Dooley, Gurnoor Singh Khurana, Chirag Mohapatra, Siddartha Venkat Naidu, and Colin White. ForecastPFN: Synthetically-trained zero-shot forecasting. In *Thirty-seventh Conference on Neural Information Processing Systems*, 2023. URL <https://openreview.net/forum?id=tScBQRNgjk>.
- Patrick Emami, Abhijeet Sahu, and Peter Graf. Buildingsbench: A large-scale dataset of 900k buildings and benchmark for short-term load forecasting. In *Thirty-seventh Conference on Neural Information Processing Systems Datasets and Benchmarks Track*, 2023. URL <https://openreview.net/forum?id=c5rqd6PZn6>.
- Rakshitha Wathsadini Godahewa, Christoph Bergmeir, Geoffrey I. Webb, Rob Hyndman, and Pablo Montero-Manso. Monash time series forecasting archive. In *Thirty-fifth Conference on Neural Information Processing Systems Datasets and Benchmarks Track (Round 2)*, 2021. URL <https://openreview.net/forum?id=wEc1mgAjU->.

- Christian D. Hubbs, Hector D. Perez, Owais Sarwar, Nikolaos V. Sahinidis, Ignacio E. Grossmann, and John M. Wassick. Or-gym: A reinforcement learning library for operations research problem. *ArXiv*, abs/2008.06319, 2020. URL <https://api.semanticscholar.org/CorpusID:221136052>.
- Thomas G. Kurtz. Solutions of ordinary differential equations as limits of pure jump Markov processes. *Journal of Applied Probability*, 7(1):49–58, 1970.
- Spyros Makridakis, Evangelos Spiliotis, and Vassilis Assimakopoulos. The m4 competition: 100,000 time series and 61 forecasting methods. *International Journal of Forecasting*, 36, 07 2019. doi: 10.1016/j.ijforecast.2019.04.014.
- Spyros Makridakis, Evangelos Spiliotis, and Vassilios Assimakopoulos. M5 accuracy competition: Results, findings, and conclusions. *International Journal of Forecasting*, 38(4):1346–1364, 2022.
- Avi Mandelbaum and Gennady Pats. State-dependent stochastic networks. Part I: Approximations and applications with continuous diffusion limits. *Annals of Applied Probability*, 8(2):569–646, 1998.
- Nachiket Naik, Prathamesh Joshi, Raj Dandekar, Rajat Dandekar, and Sreedath Panat. Bull-ode: Bullwhip learning with neural odes and universal differential equations under stochastic demand, 09 2025.
- Kashif Rasul, Arjun Ashok, Andrew Robert Williams, Arian Khorasani, George Adamopoulos, Rishika Bhagwatkar, Marin Biloš, Hena Ghonia, Nadhir Hassen, Anderson Schneider, Sahil Garg, Alexandre Drouin, Nicolas Chapados, Yuriy Nevmyvaka, and Irina Rish. Lag-llama: Towards foundation models for time series forecasting. In *R0-FoMo:Robustness of Few-shot and Zero-shot Learning in Large Foundation Models*, 2023. URL <https://openreview.net/forum?id=jYluzCLFDM>.
- Søren Taverniers, Eric J. Hall, Markos A. Katsoulakis, and Daniel M. Tartakovsky. Mutual information for explainable deep learning of multiscale systems. *Journal of Computational Physics*, 444: 110551, 2021. doi: 10.1016/j.jcp.2021.110551.
- Azmine Touseh Wasi, MD Shafikul Islam, and Adipto Raihan Akib. Supplygraph: A benchmark dataset for supply chain planning using graph neural networks. *ArXiv*, abs/2401.15299, 2024. URL <https://api.semanticscholar.org/CorpusID:267312537>.
- Duncan Watson-Parris, Yuhao Rao, Dirk Olivie, Øyvind Seland, Peer Nowack, Gustau Camps-Valls, Philip Stier, Shahine Bouabid, Maura Dewey, Emilie Fons, Jaime Gonzalez, Paula Harder, Kara Jeggle, Julien Lenhardt, Peter Manshausen, Maria Novitasari, Lucile Ricard, and Carla Roesch. ClimateBench v1.0: A benchmark for data-driven climate projections. *Journal of Advances in Modeling Earth Systems*, 14(10), 2022. doi: 10.1029/2021MS002954.
- Ward Whitt. *Stochastic-Process Limits: An Introduction to Stochastic-Process Limits and Their Application to Queues*. Springer Series in Operations Research. Springer, 2002.
- Gerald Woo, Chenghao Liu, Akshat Kumar, Caiming Xiong, Silvio Savarese, and Doyen Sahoo. Unified training of universal time series forecasting transformers. In *International Conference on Machine Learning*, 2024. URL <https://api.semanticscholar.org/CorpusID:267411817>.
- Haixu Wu et al. Time-series-library. 2024. <https://github.com/thuml/Time-Series-Library>.
- Haoyi Zhou, Shanghang Zhang, Jieqi Peng, Shuai Zhang, Jianxin Li, Hui Xiong, and Wancai Zhang. Informer: Beyond efficient transformer for long sequence time-series forecasting. 12 2020. doi: 10.48550/arXiv.2012.07436.

## A Parameter values

This appendix lists the parameter values used to produce the released runs. The algorithms that use these parameters are in §3.3.

### A.1 Demand-generator coefficients

Each item  $i$  draws its demand-process coefficients independently from the distributions of Table 5. The same distributions are used at both cardinalities  $C = 50$  and  $C = 200$ ; with shared seed, the coefficients of the first 50 items at  $C = 200$  coincide with those of the entire  $C = 50$  release. The per-item unit volume  $v_i$  used by the packing routine of §3.3.2 is drawn from  $\mathcal{U}[1.0, 4.0]$  using the same shared seed.

Table 5: Distributions of the demand-generator coefficients of Eq. (14). All coefficients are drawn once per run from the distributions below. The notation  $\mathcal{U}\{a, \dots, b\}$  denotes the discrete uniform on  $\{a, a + 1, \dots, b\}$ .

Symbol	Role	Distribution
$\bar{\lambda}_i$	baseline per-item rate	$\mathcal{U}[80, 250]$
$a_{1,i}^{(y)}$	yearly 1st-harmonic amplitude	$\mathcal{U}[0.12, 0.28]$
$a_{2,i}^{(y)}$	yearly 2nd-harmonic amplitude	$\mathcal{U}[0.04, 0.10]$
$a_i^{(w)}$	weekly amplitude	$\mathcal{U}[0.04, 0.10]$
$\phi_i, \psi_i$	seasonal phases	$\mathcal{U}[0, 2\pi]$
$\phi_i^{\text{AR}}$	AR(1) coefficient	$\mathcal{U}[0.9990, 0.9996]$
$\sigma_{\text{AR},i}$	AR(1) innovation scale	$\mathcal{U}[0.008, 0.018]$
$A_i(0)$	AR(1) initial value	$\mathcal{N}(0, 0.10^2)$
$r_i$	per-item burst rate	$\mathcal{U}[2 \cdot 10^{-4}, 10^{-3}]$
$\Delta_{i,k}^P$	per-item burst duration	$\mathcal{U}\{30, \dots, 179\}$
$h_{i,k}^P$	per-item burst height	$\mathcal{U}[0.20, 0.70]$
$N$	macro-shock event count	$\mathcal{U}\{5, \dots, 11\}$
$t_k^G$	macro-shock event start	$\mathcal{U}\{0, \dots, T - 1\}$
$\Delta_k^G$	macro-shock event duration	$\mathcal{U}\{180, \dots, 1099\}$
$h_k^G$	macro-shock event height	$\mathcal{U}[0.20, 0.60]$
$g_i$	per-item macro-shock sensitivity	$\mathcal{U}[0.4, 1.2]$

### A.2 Inventory policy and source lead times

The  $(s, S)$  levels and source lead-time means (Table 6) are configuration constants of the simulator, set per node and identical across the two releases. For each (node, item) pair the realized value is drawn once at construction as  $x = \text{base} + \mathcal{U}[-\text{var}, +\text{var}]$ , rounded to the nearest integer; clipping ensures  $0 \leq s^{n,i} < S^{n,i}$  and initial inventory lies in  $[s^{n,i}, S^{n,i}]$ . The lead-time mean  $\mu^n$  enters the source  $(s, S)$  rule only at  $n \in \mathcal{N}_{\text{src}}$ ; at intermediate nodes the realized arrival time is determined by the routing and packing of sub-steps 5–6 in Algorithm 1.

### A.3 Edge transport parameters

Each edge  $e = (u, v)$  has a transit time  $\tau_e$  in time units, a per-container volume  $V_e$  in the same units, and a per-step container count  $K_e$ , giving a per-step volume capacity  $C_e = K_e V_e$ . The two releases share  $\tau_e$  and  $K_e = 3$  on every edge;  $V_e$  scales by a factor of four on the fourteen upstream edges (Table 7). The two last-mile edges Philadelphia→NewYork and Baltimore→NewYork are back-solved at runtime; the formula is given in Appendix A.4.

### A.4 Last-mile back-solve

Let  $\bar{\lambda}$  denote the realized mean intensity of the run,  $\bar{\lambda} := (CT)^{-1} \sum_{i,t} \lambda_{i,t}$ , computed after the demand tensor is sampled. The target combined per-step volume for the two last-mile edges, with a

Table 6: Per-node inventory parameters (base  $\pm$  var) and source lead-time means  $\mu^n$ . Drawn once per (node, item) at simulator construction. “LM” marks last-mile DCs.

Node	Tier	Initial inv.	$s$	$S$	$\mu^n$ (days)
SanFrancisco	Source	4000 $\pm$ 400	400 $\pm$ 60	4000 $\pm$ 400	3 $\pm$ 1
St. Louis	Source	4000 $\pm$ 400	400 $\pm$ 60	4000 $\pm$ 400	3 $\pm$ 1
Orlando	Source	4000 $\pm$ 400	400 $\pm$ 60	4000 $\pm$ 400	3 $\pm$ 1
Nashville	Hub	8000 $\pm$ 800	1000 $\pm$ 150	8000 $\pm$ 800	3 $\pm$ 1
Atlanta	Tier-2	6000 $\pm$ 600	500 $\pm$ 80	6000 $\pm$ 600	1
Chicago	Tier-3	5000 $\pm$ 500	1000 $\pm$ 150	5000 $\pm$ 500	8 $\pm$ 1
Charlotte	Tier-3	5000 $\pm$ 500	1000 $\pm$ 150	5000 $\pm$ 500	7 $\pm$ 1
Memphis	Tier-3	3000 $\pm$ 300	500 $\pm$ 80	3000 $\pm$ 300	7 $\pm$ 1
Columbus	Tier-4	4000 $\pm$ 400	500 $\pm$ 80	4000 $\pm$ 400	2
Richmond	Tier-4	4000 $\pm$ 400	500 $\pm$ 80	4000 $\pm$ 400	2
Philadelphia	Tier-5 (LM)	3000 $\pm$ 300	500 $\pm$ 80	3000 $\pm$ 300	1
Baltimore	Tier-5 (LM)	3000 $\pm$ 300	500 $\pm$ 80	3000 $\pm$ 300	2

Table 7: Per-edge transport parameters at the two cardinalities  $C \in \{50, 200\}$ .  $\tau_e$  in time units,  $V_e$  in unit-equivalent volume,  $K_e$  per-step container count. Last-mile edges are back-solved (§A.4).

Edge	$\tau_e$	$V_e$ ( $C=50$ )	$V_e$ ( $C=200$ )	$K_e$
SanFrancisco $\rightarrow$ Nashville	4	5,000	20,000	3
St. Louis $\rightarrow$ Nashville	2	5,000	20,000	3
Orlando $\rightarrow$ Nashville	2	5,000	20,000	3
Nashville $\rightarrow$ Atlanta	1	15,000	60,000	3
Atlanta $\rightarrow$ Chicago	8	4,000	16,000	3
Atlanta $\rightarrow$ Charlotte	7	4,000	16,000	3
Atlanta $\rightarrow$ Memphis	7	4,000	16,000	3
Chicago $\rightarrow$ Columbus	2	4,000	16,000	3
Charlotte $\rightarrow$ Richmond	2	4,000	16,000	3
Columbus $\rightarrow$ Philadelphia	2	4,000	16,000	3
Richmond $\rightarrow$ Philadelphia	1	4,000	16,000	3
Richmond $\rightarrow$ Baltimore	3	3,000	12,000	3
Columbus $\rightarrow$ Baltimore	3	3,000	12,000	3
Memphis $\rightarrow$ Baltimore	2	3,000	12,000	3
Philadelphia $\rightarrow$ NewYork	1	back-solved	back-solved	3
Baltimore $\rightarrow$ NewYork	2	back-solved	back-solved	3

buffer and an allowance for wasted packing space, is

$$V_{\text{raw}} = \frac{C \bar{\lambda} \bar{v} \rho}{\eta}, \quad \bar{v} = 2.5, \rho = 1.20, \eta = 0.93, \quad (34)$$

where  $\bar{v}$  is the midpoint of the per-item volume distribution  $\mathcal{U}[1.0, 4.0]$  (used in place of the realized sample mean to keep the back-solve deterministic in the demand tensor),  $\rho$  is a target load factor giving 20% headroom above the mean, and  $\eta$  accounts for greedy first-fit waste. The split between the two edges is fixed at 0.55 : 0.45, after which each share is divided by  $K_e = 3$  and rounded to the nearest 100 to give the integer per-container volumes. The values of  $\rho$  and  $\eta$  are engineering choices, held fixed across the two releases; varying them is not part of this work.

## A.5 Runtime parameters

The two releases were produced by running the simulator script with the parameters of Table 8. All values are the script’s built-in defaults, except for the pipeline multiplier  $m$ . The default  $m = 0$  selects a reactive shipping rule that ships against backlog plus a three-time-unit buffer of smoothed demand;  $m = 7$  selects the proactive rule used in this work, which keeps seven time units of smoothed demand in the pipeline at all times.

Table 8: Runtime parameters used to produce the two releases. The pipeline multiplier  $m = 7$  is the only value that differs from the script’s defaults.

Parameter	Value
Horizon $T$	52,560
Seed	2025
Pipeline multiplier $m$	7.0 (default 0.0)
Packing	greedy first-fit
Streaming output	enabled

## B Dataset schema

### B.1 Release overview

A release contains one directory, `output_item50/` or `output_item200/`, containing six CSV files, one NumPy array, and one short text sidecar. Both releases use the same schema; they differ only in  $C$  and in the row counts of files that scale with  $C$ .

**Time index.** The time index  $t$  runs over  $\{0, \dots, T - 1\}$  with  $T = 52,560$  in both releases. Each file stores the index as an integer column named `day`; the column name reflects the resolution of the released runs (one step is one day). The simulator itself accepts any user-chosen step length, and at other resolutions the column carries the same integer index of  $t$ .

**Item identifiers.** Items are zero padded strings: I01–I50 at  $C=50$  and I001–I200 at  $C=200$ .

**Sidecar.** The release also contains `demand_signals_cols.txt`, a one-line text file listing the item identifiers in the column order used by `demand_signals.npy`.

### B.2 File inventory

Table 9 lists every file in a release, the columns that uniquely identify a row, and the number of rows or the array shape.

Table 9: File inventory of one ISOMORPH release. “Key” is the combination of columns that uniquely identifies a row. “Rows” is given as a function of the cardinality  $C \in \{50, 200\}$ , the horizon  $T = 52,560$ , and the node count  $|\mathcal{N}| = 13$ .

File	Key	Rows / shape
<code>daily_records.csv</code>	(day, item)	$T \cdot C$
<code>shipments.csv</code>	none (event log)	variable ( $3.59 \times 10^6$ at $C=50$ ; $1.35 \times 10^7$ at $C=200$ )
<code>inventory_history.csv</code>	(day, node, item)	$T \cdot  \mathcal{N}  \cdot C$
<code>backlog_history.csv</code>	(day, node, item)	$T \cdot  \mathcal{N}  \cdot C$
<code>intransit_history.csv</code>	(day, item)	$T \cdot C$ (destination only)
<code>service_summary.csv</code>	item	$C$
<code>demand_signals.npy</code>	—	$(T, C)$
<code>demand_signals_cols.txt</code>	—	1 line ( $C$ item identifiers)

### B.3 Per-file schemas

This subsection walks through each file in the order of Table 9.

`daily_records.csv`. One row per  $(t, i)$  pair, recording per-item demand and service at  $d^*$ . The two `*_end_before_ship` columns are the destination’s on-hand and backlog snapshots taken between sub-steps (4) and (5) of Algorithm 1 — after demand and service but before any dispatch. So that `served_from_stock + new_backlog_today = demand`.

`shipments.csv`. One row per dispatch committed by GREEDYPACK in sub-steps (5) and (6) of Algorithm 1. A single  $(t, \text{from}, \text{to}, i)$  combination may appear in multiple rows, since round-robin dispatch can revisit an item within the same step.

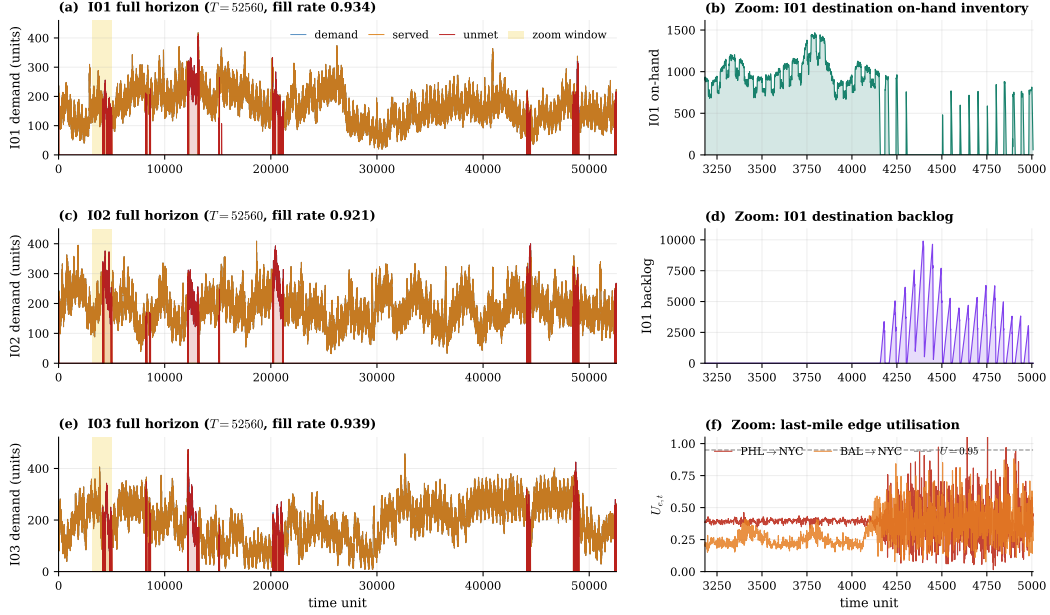


Figure 6: Baseline release at  $C=50$ , raw values at each time unit. **Left column (a, c, e)**: for items I01–I03 over the full  $T=52,560$  time units horizon, the daily demand (blue), the part served immediately from inventory at the destination (amber), and the part left unmet (red, shaded). Per-item fill rates appear in each panel’s title; the yellow band marks the zoom window shown on the right. **Right column (b, d, f)**: the network’s response for item I01 during the window around the largest demand spike — (b) inventory on hand at the destination, (d) accumulated unmet orders (backlog) at the destination, and (f) how full the two last mile edges (Philadelphia→NewYork, Baltimore→NewYork) are each day, with the  $U=0.95$  “saturation” line marked.

Table 10: Schema of `daily_records.csv`.

Column	Type	Description
<code>day</code>	int	time index $t$
<code>item</code>	str	item identifier
<code>demand</code>	int	realized demand $y_{i,t}$ (Poisson sample, Eq. 3)
<code>served_from_stock</code>	int	$\min(\text{OH}_t^{d^*,i}, y_{i,t})$
<code>new_backlog_today</code>	int	$(y_{i,t} - \text{OH}_t^{d^*,i})_+$
<code>dest_on_hand_end_before_ship</code>	int	destination on-hand right after service, before sub-step (5)
<code>dest_backlog_end_before_ship</code>	int	destination backlog right after service, before sub-step (5)

`inventory_history.csv`, `backlog_history.csv`, `intransit_history.csv`. Three long form files record the network state at the end of each step. All three share the key columns (day, node, item) of types (int, str, str) and differ only in the value column they carry (Table 12). `inventory_history.csv` and `backlog_history.csv` cover every node  $n \in \mathcal{N}$ ; `intransit_history.csv` restricts to the destination  $d^*$ , so its node column is constant. Backlog is zero at every node other than  $d^*$  by construction (§3.2.3) and is recorded as zero for schema regularity. All three values are taken at the end of step  $t$ , after all seven sub-steps of Algorithm 1 have run.

`service_summary.csv`. One row per item with five columns: `item` (str), `total_demand` (int), `served_from_stock` (int), `new_backlog_added` (int), and `fill_rate_stock_only` (float). The three integer columns aggregate the corresponding columns of `daily_records.csv` over the full horizon; the float column is `served_from_stock` divided by `total_demand`, rounded to six decimal places. The file is derived from `daily_records.csv` and included for convenience.

Table 11: Schema of `shipments.csv`.

Column	Type	Description
<code>day</code>	int	dispatch step $t$
<code>arrival_day</code>	int	arrival step at <code>to</code> , $t + \lceil \sum_{e \in P} \tau_e \rceil$
<code>from</code>	str	origin node of the dispatch
<code>to</code>	str	path endpoint
<code>item</code>	str	item identifier
<code>units</code>	int	units dispatched on this row
<code>path_nodes</code>	str	repr of <code>list[str]</code> : resolved Dijkstra path $P = (v_0, \dots, v_k)$
<code>edge_times</code>	str	repr of <code>list[float]</code> : per-edge transit times $(\tau_{e_1}, \dots, \tau_{e_k})$ in time units

Table 12: Value column of each history file. All three share the key (`day`, `node`, `item`).

File	Value column	Type	Description
<code>inventory_history.csv</code>	<code>on_hand</code>	int	on-hand inventory $\text{OH}_t^{n,i}$
<code>backlog_history.csv</code>	<code>backlog</code>	int	backlog $B_t^{n,i}$ (zero unless $n = d^*$ )
<code>intransit_history.csv</code>	<code>in_transit</code>	int	total units of item $i$ already scheduled to arrive at $d^*$ on any step after $t$ : $\sum_{\tau > t} \text{IT}_t[\tau, i]$

`demand_signals.npy`. It is a `float64` array of shape  $(T, C)$  holding the intensity values  $\lambda_{i,t}$  used to sample the demand column of `daily_records.csv` (Eq. 14); pairing samples with rates lets users study sample-versus-rate behavior without rerunning the simulator. Columns are indexed by item identifier in alphabetical order, listed comma-separated on a single line in `demand_signals_cols.txt`.

#### B.4 Scenario sweeps

The baseline release uses the default values of every scenario knob in Table 1. To study how the network’s behavior and the resulting time series change under different operating conditions, we construct six one-at-a-time sweeps: each varies a single knob across five settings—a shared baseline (all knobs at default) plus four perturbations—while holding all other knobs at baseline, producing  $6 \times 5 = 30$  rollouts on the  $C=50$  regime.

Table 13 lists all six sweeps; the baseline value is bold in each row. Three sweeps perturb the demand process and three perturb the network’s response:

- *Drift*: sets the AR(1) persistence to a single shared value  $\phi^{\text{AR}}$  across all items (Eq. 17); baseline 0.9993.
- *Shock*: multiplies the macro-shock event count  $N$  and height  $h^G$  (Eq. 19); baseline (1, 1).
- *Burst*: multiplies the per-item burst rate  $r_i$  and height  $h^P$  (Eq. 18); baseline (1, 1).
- *Edge cap*: multiplies the per-edge container count  $K_e$ ; baseline 1.
- *Buffer*: multiplies the per-node reorder thresholds ( $s, S$ ) and initial inventory; baseline 1.
- *Lead time*: multiplies the source-node mean  $\mu^n$ ; edge transit times  $\tau_e$  unchanged; baseline 1.

We select five demand-side scenarios from the six sweeps of Table 13; three are single-knob picks and two are compound scenarios that combine perturbations along multiple axes:

- `shock_xhi`: (3, 4) from the shock sweep.
- `drift_mid`:  $\phi^{\text{AR}} \in [0.95, 0.97]$  from the drift sweep.
- `burst_xhi`: (3, 4) from the burst sweep.
- `chaos_compound`: `shock_xhi` with  $\phi^{\text{AR}} \in [0.96, 0.98]$ .
- `chaos_burst`: `burst_xhi` with  $\phi^{\text{AR}} \in [0.96, 0.98]$ .

Supply-side sweeps leave the demand series unchanged and therefore cannot propagate to forecasts of  $y_{i,t}$ ; we restrict the evaluation to demand-side knobs. The evaluation protocol matches §6.1 throughout.

Table 13: The six scenario sweeps. Each sweep varies a single knob across five settings while all others stay at baseline (bold). The Type column indicates whether the sweep changes the demand process or the network’s response to it. Details of each sweep are in the text.

Sweep	Notation	Type	Settings ( <b>baseline</b> )
Drift	$\phi^{\text{AR}}$	demand	0.71, 0.86, 0.96, 0.99, <b>0.9993</b>
Shock	$(N \times h^G)$	demand	(0, 1), (0.5, 0.7), ( <b>1, 1</b> ), (2, 2), (3, 4)
Burst	$(r \times h^P)$	demand	( <b>1, 1</b> ), (1.5, 2), (2, 3), (3, 4), (5, 8)
Edge cap	$\rho_K$	supply	0.3, 0.6, <b>1.0</b> , 1.5, 2.5
Buffer	$\rho_{sS}$	supply	0.1, 0.2, 0.5, 0.75, <b>1.0</b>
Lead time	$\rho_{lt}$	supply	<b>1.0</b> , 2.0, 5.0, 10.0, 20.0

## C Foundation model evaluation details

This appendix collects the implementation details required to reproduce Table 4: the formal MASE definition (§C.1), foundation-model results at  $C=200$  (§C.2), a Lag-Llama cross-check at  $L=32$  (§C.3), per-horizon results for the five scenarios (§C.4), checkpoint identifiers and parameter counts (§C.5), and per-model inference hyperparameters (Table 18).

### C.1 MASE: formal definition

We follow the GIFT-Eval convention: the score we report is the model’s test-set MAE divided by the test-set MAE of a seasonal-naive baseline. The seasonal-naive baseline with lag 7 predicts the value from one week earlier:

$$\hat{y}_{i,t}^{\text{SN}} = y_{i,t-7}.$$

Let  $W$  be the set of rolling-origin windows and  $t_w$  the start time of window  $w$ . For a forecast  $\hat{y}^f$  produced by either the model ( $f = \text{model}$ ) or the seasonal-naive baseline ( $f = \text{SN}$ ), the cumulative MAE over the first  $h$  forecast steps, averaged across windows, is

$$\varepsilon_{i,h}^f = \frac{1}{|W|h} \sum_{w \in W} \sum_{k=0}^{h-1} |y_{i,t_w+k} - \hat{y}_{i,t_w+k}^f|.$$

The per-horizon and cross-horizon scores in Table 4 are

$$\text{MASE}(h) = \exp\left(\frac{1}{C} \sum_{i=1}^C \log \frac{\varepsilon_{i,h}^{\text{model}}}{\varepsilon_{i,h}^{\text{SN}}}\right), \quad \text{Agg.} = \exp\left(\frac{1}{|H|C} \sum_{h \in H} \sum_{i=1}^C \log \frac{\varepsilon_{i,h}^{\text{model}}}{\varepsilon_{i,h}^{\text{SN}}}\right). \quad (35)$$

The Ref. column of Table 4 uses the same formula on GIFT-Eval’s 97 tasks in place of ISOMORPH’s  $C$  items.

### C.2 Results at $C=200$

Table 14 reports the same protocol of §6.1 on the  $C=200$  release. Cells agree with the  $C=50$  Table 4 to within 0.02, as expected: with shared seed the two releases sample items from identical distributions (Appendix A.1), so additional draws do not change the per-channel geometric mean.

Table 14: Foundation models on the  $C=200$  release. Same protocol as Table 4; metric is GIFT-Eval-style MASE (Eq. 35). Best per column in **bold**.

Model	$h=1$	$h=7$	$h=14$	$h=30$	Agg.	Ref.
Chronos	0.773	0.817	0.875	1.010	0.864	0.876
Moirai	0.791	0.837	0.896	1.035	0.885	0.901
TimesFM	<b>0.741</b>	<b>0.786</b>	<b>0.843</b>	<b>0.978</b>	<b>0.832</b>	0.758
Lag-Llama	1.035	1.313	1.415	1.618	1.328	1.228

### C.3 Lag-Llama at $L=32$

The main Table 4 runs Lag-Llama at  $L=512$ , which forces a  $(L+H)/32 = 542/32 \approx 17\times$  linear RoPE rescaling on top of its  $L=32$  pre-training context. Table 15 reports the same protocol with Lag-Llama at  $L=32$ , the smallest context allowed by the  $H=30$  horizon, where the rescaling factor drops to  $62/32 \approx 2\times$  (still non-trivial because  $L+H > 32$ , but close to the no-rescaling regime the model was trained in). The aggregate MASE drops from 1.312 at  $L=512$  to 1.272 at  $L=32$ , mostly from a 0.19 improvement at  $h=30$ . The long context setting therefore explains part, but not all, of Lag-Llama’s gap to the other three models; even at  $L=32$  it is the worst of the four.

Table 15: Lag-Llama on the  $C=50$  release at  $L=32$ , same protocol as Table 4. The  $L=512$  row is reproduced from Table 4 for comparison. Rescaling factor:  $(L+H)/32$ .

Setting	rescale	$h=1$	$h=7$	$h=14$	$h=30$	Agg.
$L=512$ (Table 4)	$\approx 17\times$	1.027	1.292	1.396	1.601	1.312
$L=32$	$\approx 2\times$	1.163	1.244	1.285	1.407	<b>1.272</b>

### C.4 Per-horizon scenario results

Table 16 reports the four models on the six scenario picks at every horizon  $h \in \{1, 7, 14, 30\}$ . Two patterns visible only across horizons: (i) at  $h=1$ , the burst scenarios (burst\_xhi, chaos\_burst) score *lower* than baseline for Chronos, Moirai, and TimesFM, because most  $h=1$  windows fall outside burst events and the heightened overall demand level just normalizes the per-channel MAE downward; (ii) the model crossover (Moirai overtaking TimesFM on burst scenarios) only emerges at  $h=30$ , with TimesFM still best at  $h \in \{1, 7, 14\}$  on every burst column except chaos\_burst at  $h \in \{7, 14\}$  where Chronos edges ahead.

Table 16: Per-horizon GIFT-Eval-style MASE on the six scenario picks of Table 13. Same protocol as Table 4. Best per column within each  $h$ -block in **bold**.

Model	baseline	shock_xhi	drift_mid	chaos_comp.	burst_xhi	chaos_burst
$h=1$						
Chronos	0.769	0.779	0.761	0.768	0.638	0.643
Moirai	0.786	0.805	0.785	0.795	0.663	0.678
TimesFM	<b>0.742</b>	<b>0.748</b>	<b>0.737</b>	<b>0.743</b>	<b>0.628</b>	<b>0.638</b>
Lag-Llama	1.027	1.080	1.014	1.070	1.059	1.085
$h=7$						
Chronos	0.818	0.822	0.798	0.817	0.788	<b>0.781</b>
Moirai	0.831	0.845	0.825	0.842	0.808	0.811
TimesFM	<b>0.786</b>	<b>0.788</b>	<b>0.775</b>	<b>0.787</b>	<b>0.782</b>	0.785
Lag-Llama	1.292	1.510	1.241	1.465	1.696	1.695
$h=14$						
Chronos	0.874	0.890	0.840	0.883	0.984	<b>0.969</b>
Moirai	0.889	0.913	0.877	0.912	0.983	0.982
TimesFM	<b>0.843</b>	<b>0.854</b>	<b>0.822</b>	<b>0.851</b>	<b>0.974</b>	0.972
Lag-Llama	1.396	1.665	1.331	1.618	1.998	1.983
$h=30$						
Chronos	1.007	1.073	0.934	1.048	1.445	1.414
Moirai	1.028	1.099	0.992	1.090	<b>1.370</b>	<b>1.362</b>
TimesFM	<b>0.978</b>	<b>1.028</b>	<b>0.921</b>	<b>1.012</b>	1.399	1.384
Lag-Llama	1.601	1.974	1.503	1.916	2.406	2.367

### C.5 Models and inference hyperparameters

Table 17 lists the released checkpoint, parameter count, and pre-train context range for each model, together with the context length  $L$  used in our evaluation. Table 18 lists the inference-time hyperparameters: the number of probabilistic sample paths drawn (reduced to the per-step median for the point forecast), the batching unit each wrapper operates on, and per-model configuration knobs.

Table 17: Foundation models evaluated. Pre-train context is the sequence length used during published pre-training;  $L$  used is the context length in our zero-shot evaluation (see §6.1).

Model	HuggingFace ID	Params	Pre-train ctx	$L$ used
Chronos	amazon/chronos-t5-base	200M	512	512
Moirai	Salesforce/moirai-1.1-R-base	91M	512–2048	512
TimesFM	google/timesfm-2.0-500m-pytorch	500M	up to 2048	512
Lag-Llama	time-series-foundation-models/Lag-Llama	50M	32	512

Table 18: Inference hyperparameters. *Samples* is the number of probabilistic sample paths drawn; the per-day median is the point forecast used to compute MASE. TimesFM uses a deterministic quantile head and reports no sample count. *Batch* indicates the unit batched: Chronos and Lag-Llama batch *channels* within a window, Moirai is multivariate-native and batches *windows*, TimesFM batches *channels* per call.

Model	Samples	Batch	Model-specific
Chronos	20	channel_batch=16	bf16 inference
Moirai	100	8 ( $C=50$ ) / 1 ( $C=200$ )	patch_size=32; OOM-bound at $C=200$
TimesFM	—	per_core_batch=32	horizon_len=128 (decode 1 patch, slice to $H$ )
Lag-Llama	20	4	linear RoPE rescaling, factor $(L + H)/32$

## D Additional results

### D.1 Bullwhip method

For each non-source node  $n$  and item  $i$ , we compute Cachon’s amplification ratio Cachon et al. [2007]:

$$B_{n,i} = \frac{\text{Var}(\text{inflow}_{n,i,\cdot})}{\text{Var}(\text{outflow}_{n,i,\cdot})},$$

where  $\text{inflow}_{n,i,t}$  is the units of item  $i$  arriving at node  $n$  at time unit  $t$  and  $\text{outflow}_{n,i,t}$  is the units shipped out of  $n$  at the same time unit. At the destination, there is no downstream node; we use the realized customer demand  $y_{i,t}$  as the boundary outflow, so  $B_{\text{dest},i}$  measures how much the inbound replenishment stream amplifies the demand it is meant to serve. A ratio  $B_{n,i} > 1$  indicates the classical bullwhip signature — variability grows as one moves upstream from the customer;  $B_{n,i} = 1$  is no amplification, and  $B_{n,i} < 1$  means  $n$  smooths variability. The three source nodes (§3.2.3) replenish via a magic-stock mechanism rather than by inflow from the released network, so  $B_{n,i}$  is not defined for them and they are excluded.

Both series are aggregated into 30-time-unit totals — matching the monthly granularity at which Cachon reports bullwhip ratios — before computing variance, after dropping the first 365 time units as a warm-up. The per-node value reported in Table 3 is the mean of  $B_{n,i}$  over the  $C$  items at that node; the per-tier value is the mean over nodes in the tier.

### D.2 Per-node bullwhip ratios

Table 3 in §5.2 reports tier-level means. For reproducibility, Table 19 below gives the per-node values that those tier means are computed from. Each entry is the mean of  $B_{n,i}$  over the 50 items at node  $n$ , using the procedure described in §5.2; tier names match Table 6.

### D.3 Additional results on Forward UQ

## E Computational resources

**Time-series generation.** Simulator runs are CPU-only and single-core. A  $C=50$  rollout takes roughly 20 minutes;  $C=200$  roughly 90 minutes. The release adds up to 48 newly generated rollouts: the  $C=50$  and  $C=200$  baselines, 26 perturbed named scenarios at  $C=50$  from §5 (the six sweeps contribute four non-baseline settings each,  $4 \times 6$ , plus the two compound scenarios chaos\_compound

Table 19: Per-node bullwhip ratio  $\bar{B}_n$  on the  $C=50$  release. Each value is the mean over the 50 items at that node; the same numbers averaged within tier appear in Table 3. The wide spread between Baltimore and Philadelphia in the daily column reflects sub-monthly batching of arrivals, which the monthly column smooths out.

Node	Tier	Daily $\bar{B}_n$	Monthly $\bar{B}_n$
NewYork	Destination	9.03	1.43
Baltimore	Tier-5	6.83	1.64
Philadelphia	Tier-5	19.16	1.49
Columbus	Tier-4	1.39	1.27
Richmond	Tier-4	1.40	1.34
Charlotte	Tier-3	1.15	1.33
Chicago	Tier-3	1.07	1.17
Memphis	Tier-3	1.27	1.21
Atlanta	Tier-2	1.29	1.16
Nashville	Hub	0.97	1.07

and `chaos_burst`; the per-sweep baseline is shared with the main  $C=50$  release rather than re-simulated), and the 20 LHS UQ perturbations of §6.2. Wall-clock on the order of 20 CPU hours.

**Foundation-model inference.** All zero-shot inference ran on a single NVIDIA RTX 2080 Ti, one job per GPU. The pipeline covers 109 jobs: 29 for the TSF evaluation of §6 (4 models  $\times$  2 baselines + 4 models  $\times$  5 demand-side scenarios + 1 Lag-Llama  $L=32$  cross-check) and 80 for the forward-UQ ensemble of §6.2 (4 models  $\times$  20 LHS perturbations). Aggregate wall-clock is on the order of 30 GPU hours: roughly 22 hours for the TSF evaluation (each job runs the full  $|W|=262$  rolling-origin protocol of §6 at stride 30) and roughly 7 hours for the UQ ensemble (each UQ job evaluates only the windows used,  $|W|=50$  at stride 150,  $\sim 5$  minutes per job).

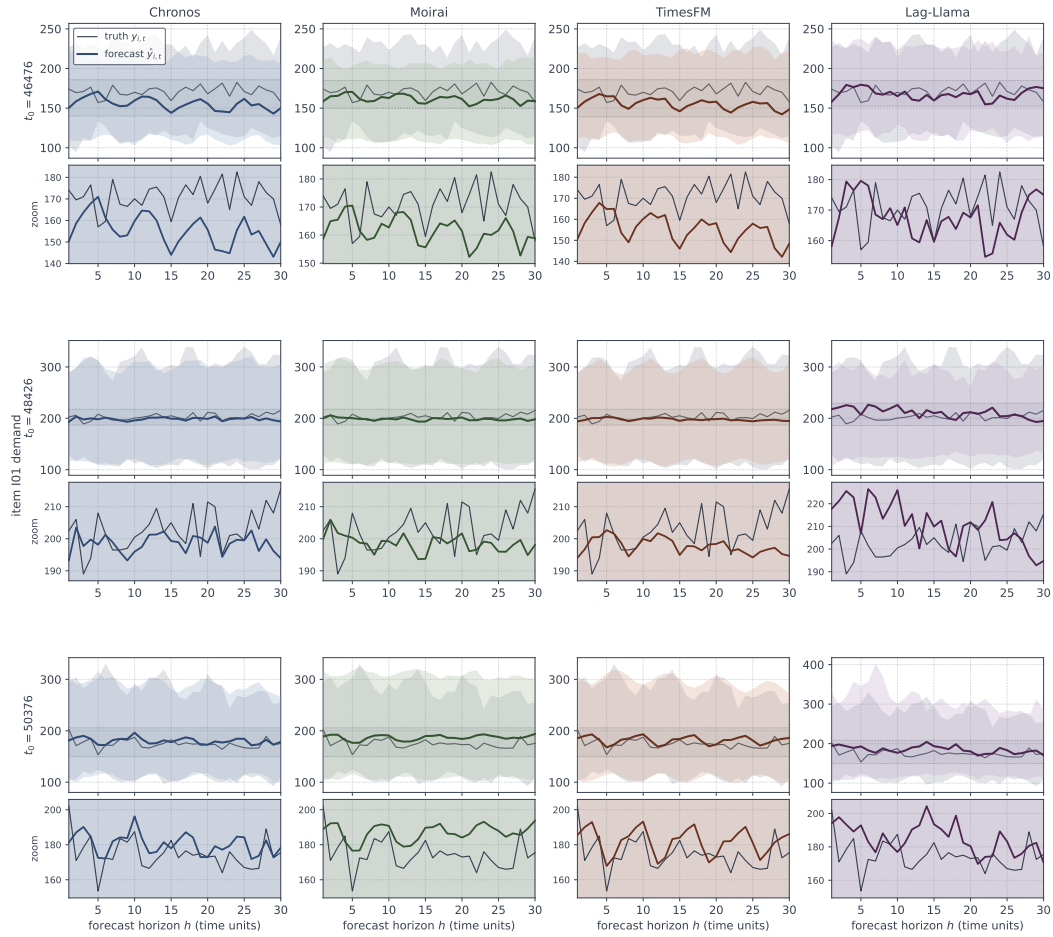


Figure 7: Forward UQ forecast envelopes for item I01 at three forecast windows ( $t_0 = 46,476$ ,  $48,426$ ,  $50,376$ ). Each column is one foundation model; each row pair shows the full envelope and a zoom into the median region. Setup matches Figure 5.